LUND UNIVERSITY

# alpha-Synuclein expression and Nrf2 deficiency cooperate to aggravate protein aggregation, neuronal death and inflammation in early-stage Parkinson's disease

Lastres-Becker, Isabel; Ulusoy, Ayse; Innamorato, Nadia G.; Sahin, Gurdal; Rabano, Alberto; Kirik, Deniz; Cuadrado, Antonio

*Published in:*
Human Molecular Genetics

*DOI:*
10.1093/hmg/dds143

2012

Link to publication

*Citation for published version (APA):*
Lastres-Becker, I., Ulusoy, A., Innamorato, N. G., Sahin, G., Rabano, A., Kirik, D., & Cuadrado, A. (2012). alpha-Synuclein expression and Nrf2 deficiency cooperate to aggravate protein aggregation, neuronal death and inflammation in early-stage Parkinson's disease. *Human Molecular Genetics*, *21*(14), 3173-3192. https://doi.org/10.1093/hmg/dds143

*Total number of authors:*
7

**General rights**
Unless other specific re-use rights are stated the following general rights apply:
Copyright and moral rights for the publications made accessible in the public portal are retained by the authors and/or other copyright owners and it is a condition of accessing publications that users recognise and abide by the legal requirements associated with these rights.
• Users may download and print one copy of any publication from the public portal for the purpose of private study or research.
• You may not further distribute the material or use it for any profit-making activity or commercial gain
• You may freely distribute the URL identifying the publication in the public portal

Read more about Creative commons licenses: https://creativecommons.org/licenses/

**Take down policy**
If you believe that this document breaches copyright please contact us providing details, and we will remove access to the work immediately and investigate your claim.

LUND UNIVERSITY

PO Box 117
221 00 Lund
+46 46-222 00 00

Download date: 09. Dec. 2025

# α-Synuclein expression and Nrf2-deficiency cooperate to aggravate protein aggregation, neuronal death and inflammation in early-stage Parkinson's disease

Isabel Lastres-Becker[1*], Ayse Ulusoy[2,3], Nadia G. Innamorato[1], Gurdal Sahin[2], Alberto Rábano[4], Deniz Kirik[2] and Antonio Cuadrado[1*]

[1] Centro de Investigación en Red sobre Enfermedades Neurodegenerativas (CIBERNED). Instituto de Investigación Sanitaria La Paz (IdiPAZ). Departamento de Bioquímica e Instituto de Investigaciones Biomédicas "Alberto Sols" CSIC-UAM, Facultad de Medicina, Universidad Autónoma de Madrid.

[2] Department of Experimental Medical Science, Brain Repair and Imaging in Neural Systems, Lund University, Lund, Sweden

[3] German Center for Neurodegenerative Diseases (DZNE), Bonn, Germany

[4] Department of Neuropathology and Tissue Bank, Unidad de Investigación Proyecto Alzheimer, Fundación CIEN, Instituto de Salud Carlos III, Madrid, Spain

[*]Correspondence to:
Prof. Dr. Antonio Cuadrado and Dr. Isabel Lastres-Becker
Departamento de Bioquímica
Instituto de Investigaciones Biomédicas "Alberto Sols"
CSIC-UAM
C/Arturo Duperier 4
28029 Madrid
Spain
Tel: +34 91 585 4383 and Fax: +34 91 585 4401
E-mail: antonio.cuadrado@uam.es; ilbecker@iib.uam.es

**ABSTRACT**

Although α-synucleinopathy is a hallmark of sporadic and familial Parkinson's disease (PD), it is not known how α-synuclein (α-SYN) contributes to early events in PD pathogenesis. Here we demonstrate that α-SYN overexpression and Nrf2 deficiency cooperate to worsen protein aggregation, neuronal death and inflammation in a new animal model of PD based on stereotaxic delivery of an adeno-associated viral vector (rAAV) for expression of human α-SYN in ventral midbrain of Nrf2 knockout mice ($Nrf2^{-/-}$). Two months after surgery $Nrf2^{-/-}$ mice exhibited exacerbated degeneration of nigral dopaminergic neurons, increased dystrophic dendrites, reminiscent of Lewy neurites, and impaired proteasome gene expression and proteasome activity. Dopaminergic neuron loss correlated with an increase in neuroinflammation and gliosis and Nrf2-deficiency intensified reactive gliosis at the ventral midbrain. In response to α-SYN, $Nrf2^{-/-}$ microglia failed to activate the expression of two anti-inflammatory genes heme oxygenase-1 (HO-1) and NADPH quinone oxidorreductase-1 (NQO1). The impairment in Nrf2 response correlated with a shift in the microglial activation pattern, towards increased production of pro-inflammatory markers, IL-6, IL-1β and iNOS, reduced phagocytic capacity of fluorescent beads and lower messenger RNA levels for TAM receptors Axl and Mer. Postmortem brain tissue samples from patients in early to middle-stage progression of PD showed increased HO-1 expression in astrocytes and microglia suggesting an attempt of the diseased brain to compensate excessive production of reactive oxygen species and inflammation. This study demonstrates that α-SYN and Nrf2 deficiency cooperate on protein aggregation, neuroinflammation and neuronal death, and provide a bi-factorial animal model to study early-stage Parkinson's disease.

## INTRODUCTION

The causes that lead to Parkinson's disease (PD) remain largely unknown but a strong correlation exists between the extent of the neurodegeneration and the amount, structure, subcellular location and function of α-synuclein (α-SYN). In idiopathic PD, α-SYN accumulates in Lewy bodies and dystrophic neurites, which are thought to be the underlying pathology leading to neurodegeneration and are related to the onset and progression of clinical symptoms (1). Three point mutations (A53T, A30P and E46K) in the α-SYN gene as well as duplication and triplication of the wild type gene have been found to cause a familial form of PD (2, 3). Although its exact role in neuron physiology and pathology is ill defined, evidence suggests that overexpression of wild type or the above mentioned point mutations of α-SYN might lead to a toxic gain of function related to alterations in axonal transport, oxidative stress (4-6) and neuroinflammation (7-10).

Unfortunately, most animal models used to study PD, such as MPTP and other toxin-based models, do not faithfully reproduce the α-synucleinopathy of PD and therefore they have a limited value to understand the human pathology and to develop disease modifying therapies (11). As a result, some observations made in these neurotoxin models might be misleading. For example, GDNF administered either as recombinant protein or via viral vectors has been found to be highly efficient in protecting nigral DA neurons from neurodegeneration induced by MPTP or 6-OHDA (12-14), while it has failed to provide any protection against α-SYN overexpression (15, 16).

In recent years, new PD models have been developed which are based on overexpressing human α-SYN in the rodent midbrain by means of stereotaxic delivery of an adeno-associated viral expression vector (rAAV), serotype 6 in our case (17, 18).

These models reproduce important aspects of human PD such as axonal pathology and inflammatory changes, they develop slowly and progressively and lead to α-SYN-positive cytoplasmic inclusions (19). The morphology of α-SYN-containing dystrophic axons is remarkably similar to those observed in brains from PD patients (20, 21). The rAAV6-α-SYN model is characterized by a mild loss of tyrosine hydroxylase (TH)-positive neurons in the SN in the range of 50% in rats (18) and 20-25% in mice as observed at 2-3 months after injection, (22). Therefore, this slow and progressive model suggests that α-SYN overexpression may require at least one additional hit to enhance α-synucleinopathy and induce more robust neuroanatomical alterations. Such hit may include the induction of a more prominent or long-lasting inflammatory response.

We and others have demonstrated that Nrf2 modulates microglial activation to prevent an excessive anti-inflammatory response in the MPTP mouse paradigm (23-25). Nrf2 regulates the cell response against oxidative and inflammatory stress and controls the expression of more than 100 genes involved in antioxidant and detoxification reactions including those coding for heme oxigenase-1 (HO-1), NAD(P)H quinone reductase 1 (NQO1) and enzymes related to glutathione metabolism such as glutathione S-transferase, γ-glutamil cystein ligase, glutathione peroxidase, glutathione reductase, etc (26). Therefore, in this study we have built on the hypothesis that Nrf2-deficiency might sensitize mice to proteinopathy and provide the "second hit" for enhanced neuroinflammation. Indeed, several evidences suggest a very relevant role of this transcription factor or its target phase 2 genes in the development of PD. Thus, Nrf2 was strongly expressed in the nucleus of the surviving nigral neurons in PD (27), indicating that Nrf2 was induced, but maybe it was insufficient to protect neurons from degeneration. More recently, an association was found between an haplotype in the Nrf2-codifying NFE2L2 gen, including the promoter, and risk to develop of PD (28,

29). Overall, these data demonstrate that there is a strong relationship between PD and Nrf2, although it remains to be determined if impairment of Nrf2 cooperates with α-SYN pathology overexpression and Nrf2 implication in the progression of the disease.

Therefore, in this study we have analyzed the main hallmarks of human PD in Nrf2-knokcout mice submitted to stereotaxic delivery of AAV6-α-SYN in the ventral midbrain. We report that α-SYN overexpression as primary insult and Nrf2 deficiency as sensitive background cooperate to worsen protein aggregation, neuronal death and neuroinflammation.

## RESULTS

*Genetic deletion of the transcription factor Nrf2 aggravates nigral dopaminergic cell death elicited by α-SYN over-expression.*

First we developed a PD mouse model based on combination of α-SYN overexpression and impaired Nrf2 response, achieved by stereotaxic delivery of a recombinant adeno-associated vector for expression of human α-SYN (rAAV6-α-SYN) in the ventral midbrain of Nrf2 knockout mice. Two µl of viral vector (at 4.0 x $10^{12}$ GC/ml) were injected into the right ventral midbrain, just dorsal to the location of SN in either $Nrf2^{-/-}$ or $Nrf2^{+/+}$ littermates. Mice of both genotypes selected for this study expressed the rAAV6-encoded transgene with somewhat similar efficiency in the striatum and ventral midbrain as determined with an antibody against human α-SYN. However, there was a tendency to see fewer α-SYN-stained neurons in $Nrf2^{-/-}$, already anticipating higher neuron loss in this genetic background as a result of α-SYN toxicity (Fig. 1A). Double-immunofluorescence staining indicated that most cells expressing human α-SYN were also labelled with anti-TH antibodies, therefore confirming the expression of this rAAV6-α-SYN vector in nigral DAergic neurons (Fig. 1B).

Moreover, human α-SYN was anterogradely transported to the striatum along the nigrostriatal fiber projections in both mouse groups (Fig. 1C). Similar results were obtained with a rAAV6 vector expressing green fluorescence protein (GFP) (data not shown). These results are in agreement with previous work published using these vectors (30-32) and validate these genotypes as a model to compare the role of Nrf2 in α-synucleinopathy.

We evaluated DAergic neuron death in those animals at 8 weeks after injection, which corresponds to the time point when neuropathological findings in this model of slow PD progression are intense (15, 17, 18). At this dose, injection of rAAV6-α-SYN induced a small reduction of nigral DAergic neurons in the injected right side in comparison with the non-injected left side in $Nrf2^{+/+}$ mice as determined by immunohistochemical staining of $TH^{+}$ neurons (Fig. 2A). By contrast, in $Nrf2^{-/-}$ mice we observed exacerbated loss of $TH^{+}$ neurons (Fig. 2B), which was accompanied by increased loss of dendritic fibers at the ventral side of SN (Fig. 2C and 2D). Stereological analyses corroborated these observations indicating that $Nrf2^{-/-}$ mice showed 23% greater nigral DAergic neuron loss then $Nrf2^{+/+}$ mice (Figure 2I).

We found similar striatal $TH^{+}$ fiber staining at the injected and non-injected sides of both $Nrf2^{+/+}$ and $Nrf2^{-/-}$ mice, as detected by immunohistochemistry (Fig. 2E, 2F, 2G and 2H) and immunoblot of striatal protein lysates with anti-TH antibodies (Suppl. Fig. 1). These results were somewhat unexpected because there was α-SYN anterograde expression in the striatum (Fig. 1C). In addition, in $Nrf2^{-/-}$ mice striatal DA exhibited only a minor non-significant decrease in the lesioned side compared to the non-lesioned side (as shown in Fig. 2J). DOPAC, a major DA metabolite, and the ratio DOPAC/DA, indicative of DA turnover, did not show a statistically significant difference, although there was a trend of increase in the α-SYN overexpressing $Nrf2^{-/-}$

mice (Fig. 2K and 2L). Homovanillic acid levels did not show a significant difference either (data not shown). Consistent with these observations, we did not observe a behavioral motor asymmetry between lesioned and non-lesioned groups when they were submitted to the corridor test (33) or to the standard apomorphine test (data not shown). These results suggest that surviving DAergic neurons might sprout to maintain efferent fiber density at sufficiently high levels to compensate for the small neuronal loss (34). To determine if there are plasticity-related changes, we performed immunofluorescence staining for synapthophysin, as a synaptic marker, in the striatum (35). Animals showed increased expression of synaptophysin in the side injected with rAAV6-α-SYN, in comparison with the rAAV6-GFP injected controls (Suppl. Fig. 2). While these results suggest that this model is particularly useful to study early stages of parkinsonian neurodegeneration, where there is still limited neurondegeneration but at the same time, the fact that there was more sensibility to α-SYN toxicity in the SN of $Nrf2^{-/-}$ mice also suggests the importance of this transcription factor in protection against α-synucleinopathy.

*$Nrf2^{-/-}$ mice exhibit an exacerbated aggregation of α-SYN in dendrites and mild reduction of proteasome subunits.*

Overexpressed α-SYN accumulated densely in DAergic fibers of both genotypes. However, $Nrf2^{-/-}$ mice exhibited many thick dendrites that were heavily loaded with α-SYN (Fig. 3B) compared to $Nrf2^{+/+}$ mice (Fig. 3A). This pathologic accumulation of α-SYN was similar to that observed in dystrophic Lewy neurites found in PD patients (Fig. 3C). These results are in line with the notion that α-SYN degradation is a limiting step in PD pathology but, more importantly, they highlight the relevance of Nrf2 in proteostasis.

One possible cause for α-SYN aggregation is impairment in the ubiquitin-proteasome system. In an in silico analysis, we identified putative Nrf2-regulated Antioxidant Response Elements (AREs) in the promoters of several proteasome subunits (data not shown). This analysis was further supported by analysis of available data from published microarrays (data not shown). Therefore, to clearly determine if Nrf2 migth regulate the expression of proteasome genes we measured mRNA levels of some proteasome subunits in mouse embryofibroblasts (MEFs) obtained from $Nrf2^{+/+}$ and $Nrf2^{-/-}$ mice. MEFs from $Nrf2^{-/-}$ mice exhibited lower basal mRNA levels of subunits PSM B7, C3 and C4 (Suppl. Fig. 4A) although the difference was too small to be detected by immunoblot (data not shown). In response to the proteasome inhibitor MG132, which stabilizes Nrf2 protein levels and also stimulates expression of protesome genes (36), we found that $Nrf2^{-/-}$-derived MEFs consistently showed an impaired increased in mRNA of those subunits compared to $Nrf2^{+/+}$-derived MEFs (Suppl. Fig. 4A). Moreover, proteasome enzymatic chymiotrypsin and peptidylglutamyl peptide hydrolysing (PGPH) activities were lower in extracts from $Nrf2^{-/-}$ MEFs than in control ones (Suppl. Fig. 4B).

Based on those observations, we analyzed the messenger RNA levels of PSMC3, PSMC4 and PSMB7 which are changed in PD patients (37-39). The three mRNAs exhibited a lower basal abundance in $Nrf2^{-/-}$ compared to $Nrf2^{+/+}$ mice although the difference did not reach statistical significance (Fig. 3D). To study more specifically the α-SYN-challenged neurons, we analyzed by immunohistochemistry the protein levels of PSMB7 (Fig. 3E). All neurons that over-expressed α-SYN presented positive puntacte expression of PSMB7, although not all cells that expressed PSMB7 were α-SYN positive. Interestingly, in $Nrf2^{-/-}$ mice the induction of PSMB7 was drastically impaired in comparison to $Nrf2^{+/+}$ mice. These results suggest that proteasomal adaptation to

process high levels of α-SYN is impaired in Nrf2$^{-/-}$ mice, resulting in α-SYN accumulation in dystrophic neurites. When we looked at the basal expression of PSMB7 in mice injected with rAAV6-GFP we observed that Nrf2$^{-/-}$ mice expressed less PSMB7 in comparison to their wild-type littermates (Suppl. Fig 3).

Interestengly, α-SYN is phosphorylated at S$^{129}$ in neuropathological lesions. Moreover, this phospho-S$^{129}$-α-SYN is preferentially distributed to swollen neurites and the nucleus (40). Although the exact role of phospho-S$^{129}$-α-SYN remains unclear, the proteasome pathway may play a role in the accumulation of Ser$^{129}$-phosphorylated α-SYN, which is particularly abundant in PD brains (41). So, we further pursued the effect of proteasomal impairment by analyzing the phosphorylation state of α-SYN. Immunofluorescence analysis detected phospho-S$^{129}$-α-SYN only at the side of the SN that had been injected with rAAV6-α-SYN. We did not find positive staining at either the rAAV6-GFP injected or the non-injected sides (data not shown). When we compared the phospho-S$^{129}$-α-SYN staining between Nrf2$^{+/+}$ and Nrf2$^{-/-}$ mice we detected significantly enhanced staining in Nrf2$^{-/-}$ neurons (Fig. 4). Taken together these results indicate that α-synucleinopathy is aggravated in Nrf2$^{-/-}$ mice due at least in part to impaired regulation of some proteasome genes.

*α-SYN overexpression worsens glial activation at the SN of Nrf2$^{-/-}$ mice.*

Next, we analyzed the effect of Nrf2 deficiency on the profiles of astroglial and microglial activation in response to α-SYN. Double immunofluorescence with anti-α-SYN and anti-GFAP antibodies in 30 μm-thick coronal midbrain sections demonstrated astrocyte activation in both mouse genotypes. Nrf2$^{-/-}$ mice exhibited more astrocytes than Nrf2$^{+/+}$ littermates in the area of α-SYN overexpression at the SN. These astrocytes displayed enlarged bodies and ramifications consistent with activation (Fig. 5A).

Quantification of these morphological changes showed that Nrf2$^{-/-}$ mice presented increased number of B-type astrocytes (Fig. 5B). Regarding microglia, double immunofluorescence with anti-α-SYN and anti-Iba1 antibodies indicated that Nrf2$^{-/-}$ microglia displayed enlarged bodies with pseudoameboid shape in the area of α-SYN overexpression at the SN in comparison to the Nrf2$^{+/+}$ microglia (Fig. 5C). We differentiated four microglial states: type A: resting microglia; type B: initiation of microglial activation; type C: activated but non-phagocytic; type D: activated phagocytic (42). Quantification of the different activation states of microglial cells showed that in the Nrf2$^{-/-}$ mice there was an increased in type B and C states, indicating exacerbated microglial activation (Figure 5D). Glial changes were attributed to α-SYN expression because injection of a rAAV6-GFP control vector did not lead to reactive astrogliosis or microgliosis at the same area (Fig. 5A and 5B). Interestingly, we observed that Nrf2$^{-/-}$ mice presented increased baseline number of microglial cells, as previously reported (24) suggesting in agreement with pr.that these animals have already aincresed baselene leves of inflalmtion. Taken together these results indicate that Nrf2-deficiency aggravates the gliosis caused by α-SYN overexpression in the surrounding area of degeneration.

*Impaired uptake of α-SYN and increased pro-inflammatory markers in Nrf2$^{-/-}$deficient astrocytes*

To determine if glial changes might be a consequence of α-SYN stimulation rather than just a mere consequence of neuron damage, we analyzed the effect of recombinant α-SYN on glial cultures. Immunocytochemistry analysis demonstrated that neither Nrf2$^{+/+}$ nor Nrf2$^{-/-}$ astrocytes expressed α-SYN at basal levels (Fig. 6). Most cultured astrocytes from both Nrf2$^{+/+}$ and Nrf2$^{-/-}$ mice exhibited a flat polygonal or

spindle-like, morphology as expected (43). Upon treatment with 1 μM α-SYN for 8 h, both astrocyte types showed α-SYN$^{+}$ inclusion bodies and some cells rounded and condensed (Fig. 6). These data indicate that α-SYN is somehow internalized by astrocytes in agreement with (44), but there is no clear difference between both genotypes. In order to determine if α-SYN could just adhere non-specifically to astrocytes, we compared the effect of adding monomeric and oligomeric α-SYN to astrocytes. Confocal microscopy showed that monomeric α-SYN was inside the astrocyte (Fig. 5), however oligomeric α-SYN was attached to the cell surface (Suppl. Fig. 5). Hence, we conclude that monomeric α-SYN is taken by astrocytes from both genotypes. In response to α-SYN, there was not induction of phase 2 enzymes like HO-1 or NQO1 (Fig. 7A and 7B), and Nrf2$^{+/+}$ astrocytes released low levels of pro-inflammatory cytokines IL-6, IL-1β and iNOS that were slightly higher in Nrf2$^{-/-}$ astrocytes (Fig. 7C, 7D and 7E, respectively). When we analyzed anti-inflammatory cytokines like IL-4, Nrf2$^{-/-}$ astrocytes exhibited about 50% less baseline expression than Nrf2$^{+/+}$ astrocytes (Fig. 7F) and treatment with α-SYN decreased progressively its levels in the Nrf2$^{+/+}$ astrocytes, indicating that α-SYN decreased the anti-inflammatory capacity of astrocytes. Taken together, these data indicate that, contrary to the *in vivo* model where Nrf2$^{-/-}$ mice exhibited enhanced astrogliosis, in culture α-SYN is taken up and activates astrocytes of both genotypes to a similar extent (see Discussion).

*α-SYN activates the NF-κB and Nrf2 pathways.*

To determine whether α-SYN induces microglial activation and the pathways implicated, we first used the microglial cell line BV2. We focused on the crosstalk between p65-NF-κB and Nrf2, which are master regulators of pro-inflammatory (iNOS, IL-1β, IL-6 and others) and anti-oxidant phase 2 (HO-1, NQO1 and others) genes,

respectively. α-SYN increased p65 protein levels in a time-dependent manner and reached a maximum after 30 min (Fig. 8A and 8B). Similarly, α-SYN also increased Nrf2 protein levels following 2 h after treatment (Fig. 8A and 8B). In addition, α-SYN treatment for 4 and 8 h induced the mRNA expression of HO-1, a prototype Nrf2-regulated phase 2 gene, and IL-1β, IL-6 and iNOS, all targets of NF-κB (Fig. 8C). At the protein level, α-SYN required 8 h to increase HO-1, although iNOS and Iba-1 were already induced by 4 h (Fig. 8D and 8E). These data indicate that α-SYN activates the NF-κB pro-inflammatory pathway in the short-term and the Nrf2 anti-inflammatory pathway in a longer term.

*Nrf2-deficiency alters microglial morphology and pro-inflammatory cytokine production in response to α-SYN.*

In order to get more insight on the function of Nrf2 in the microgliosis caused by α-SYN overexpression, we analyzed the effect of α-SYN in primary microglia from $Nrf2^{+/+}$ and $Nrf2^{-/-}$ mice. Immunofluorescence analysis demonstrated that at basal levels $Nrf2^{+/+}$-derived microglia expressed α-SYN, which corroborates previous findings (10) and $Nrf2^{-/-}$ microglia did not present any apparent alteration in endogenous α-SYN expression (Fig. 9). When $Nrf2^{+/+}$ microglia was exposed to α-SYN (1 μM, 8h) we observed a progressive transition from the rod-shaped to the ameboid morphology (Fig. 9). Interestingly, $Nrf2^{-/-}$ microglia presented an ameboid shape and vacuolated cytoplasm with some spine-like structures and in some cells there was a tendency to become round and condensed. To determine the mechanism of interaction of α-SYN and microglial cells, we analysed in uptake of monomeric and oligomeric α-SYN. Confocal microscopy showed that monomeric α-SYN was inside the microglia (Fig. 9), while oligomeric α-SYN was just adhered to the cell surface (Suppl. Fig. 6).

To further define the modulatory role of Nrf2 in the microglial inflammatory response to α-SYN, we determined by qRT-PCR mRNA levels of HO-1 and NQO1, which are regulated by Nrf2. Untreated $Nrf2^{-/-}$ microglia expressed lower basal levels of both enzymes than $Nrf2^{+/+}$ microglia, as expected (Fig. 10A and 10B). When $Nrf2^{+/+}$ microglia was treated with α-SYN, there was an increase in mRNA levels of both HO-1 and NQO1 after 8 h but not in $Nrf2^{-/-}$ microglia (Fig. 10A and 10B). Furthermore, we analyzed mRNA levels of pro-inflammatory cytokines IL-6 and IL-1β and iNOS. In $Nrf2^{+/+}$ microglia, these factors reached maximal levels at 4 h and were maintained for at least 8 h, but in the case of $Nrf2^{-/-}$ microglia, these pro-inflammatory factors continued to rise even after 8 h (Fig. 10C, 10D and 10E), indicating that Nrf2 modulates the pro-inflammatory response to α-SYN in microglia.

To study the phagocytic response to α-SYN, microglia from $Nrf2^{+/+}$ and $Nrf2^{-/-}$ mice were incubated for 2 h with fluorescent-labeled polystyrene beads in absence or presence of 1 μM α-SYN. Phagocytic activity was measured as a function of the amount of intracellular beads (Fig. 10F). At basal levels $Nrf2^{-/-}$ microglia showed impaired phagocytosis compared to $Nrf2^{+/+}$ cells. α-SYN enhanced phagocytosis in $Nrf2^{+/+}$ and $Nrf2^{-/-}$ microglia, although the $Nrf2^{-/-}$ microglia was less efficient (Fig. 10F). It has been reported that TAM receptor tyrosine kinases, Axl, Mer and Tyro3, are implicated in microglial phagocytosis and inflammatory gene expression (45). Interestingly at basal levels, Nrf2-deficiency significantly decreased mRNA levels of Axl (Fig. 10G) and Mer (Fig 10H) while the change on Tyro3 was not statistically significant (Fig. 10I). When microglial cells were treated with α-SYN, the Axl receptor showed a diminished induction in $Nrf2^{-/-}$ microglia, compared to $Nrf2^{+/+}$. These results suggest that Nrf2 deficiency impairs microglial phagocytosis and provide an explanation to the

observation reported in Fig. 9, indicating that $Nrf2^{+/+}$ had greater α-SYN aggregates than $Nrf2^{-/-}$ microglia.

Taken together, these data indicate that α-SYN induced the activation of the Nrf2 pathway in microglia, and that Nrf2 participates in the acquisition of both pro- and anti-inflammatory phenotypes of microglia, favoring its scavenging over its inflammatory role.

*Evidence for phase 2 induction at the SN pars compacta in human PD*

To determine the relevance of phase 2 enzymes in modulation of inflammation in Parkinson's disease, we compared the levels of HO-1 in biopsies from asymptomatic subjects and patients with α-synucleinopathy in a medium stage of PD progression (Braak stages 4-5). In PD patients with α-synucleinopathy, demonstrated by formation of Lewy bodies and dystrophic Lewy dendrites (data not shown), we analyzed co-expression of both HO-1 and either GFAP for astrocytes or Iba1 for microglia, compared to control asymptomatic patients. It was not possible to perform double labeling due to different retrieval requirements for each antigen, HO-1, GFAP and Iba-1, but we circumvented this problem by analyzing two adjacent 4-µm thick sections that in many cases showed part of the same cells. As shown in Fig. 11B, PD tissue showed increased astro- and microgliosis compared to control tissue (Fig. 11A). At higher magnification, we observed that some activated astrocytes with thick bodies and branches evidenced by GFAP staining were also positive for HO-1 staining in PD tissue (Fig.11C and 11 D) . Similarly, some clusters of Iba1-stained microglia were also positive for HO-1 expression (Fig. 11E and 11F). We quantified these observations in inmunoblots of human tissue from the SN comparing control versus PD patients. Enhanced HO-1 protein levels were observed in PD patients which correlate with

increased expression of GFAP and Iba1 (Fig. 12), indicating that reactive astrogliosis and microglial activation was accompanied by augmented levels of enzyme HO-1. These results suggest that some glial cells up-regulate the phase 2 response possibly in an attempt to modulate the oxidative stress and inflammation that result at least in part from α-SYN interaction with glia.

## DISCUSSION

This study demonstrates that impairment of Nrf2 response cooperates with α-SYN overexpression to aggravate the hallmarks of PD including proteinopathy, inflammation and nigrostriatal cell death, and provides a new more complete bifactorial mouse model based on α-SYN and Nrf2 paradigms to study early stages of PD and to develop new therapeutic strategies. The study of α-synucleinopathy and its contribution to PD ethiopathology has been hampered due to the lack of reliable animal models. The recent use of AAV vectors for α-SYN expression has provided a powerful new tool to reassess the contribution of proteinopathy, axonal dysfunction, neuron cell death, oxidative stress and neuroinflammation in PD. Moreover, the slow and progressive development of this animal model provides an excellent ground to analyze the cooperation of other factors that may participate in disease initiation and progression. In this study, we have analyzed the relevance of impaired Nrf2 transcriptional activity as an adjuvant factor in disease progression. We have found that Nrf2 deficiency aggravates α-SYN aggregation in neuronal bodies and dystrophic neurites, gliosis, inflammation and DAergic neuron death.

Several preliminary studies including ours have demonstrated the importance of Nrf2 in protections against oxidative and inflammatory stress in mice treated with the parkinsonian toxin 1-methyl-1,2,3,4-tetrahydropyridine (MPTP) (24, 25, 46-48).

However, the MPTP model does not recapitulate the main hallmark of the human PD pathology which is α-synucleinopathy. Therefore, we undertook this study with two main goals: i) to generate a better mouse model that combines α-SYN pathology and predisposition to oxidative and inflammatory stress ii) to determine in this model how relevant Nrf2 might be to control proteostasis following α-SYN challenge. Here we have observed that Nrf2-deficieny aggravates neuronal death, gliosis and inflammation in this scenario but also proteinopathy associated with α-SYN accumulation in neuron bodies and dystrophic neurites.

To our knowledge this is the first study where proteinopathy associated with PD is analyzed in connection with Nrf2-deficiency. Basal mRNA levels of several proteasome subunits like PSMB7, PSMC3 and PSMC4 were slightly decreased in ventral midbrain of $Nrf2^{-/-}$ mice compared to $Nrf2^{+/+}$ mice. Moreover, $Nrf2^{-/-}$-derived MEFs treated with the proteasome inhibitor MG132, which stabilizes Nrf2 protein levels and also stimulates expression of protesome genes (36), showed impaired expression of proteasomal genes and proteasome catalytic activity compared to $Nrf2^{+/+}$-derived MEFs. The fact that $Nrf2^{-/-}$ mice exhibited impaired proteasome gene expression and activity provides an interpretation to the reported decrease of proteasome activity and low levels of 20S and 26S subunits in PD brains (49-51). Microarray studies (52, 53) indicate that several 20S and 26S protesomal subuntis might be transcriptionaly up-regulated by Nrf2 and Kensler's group has reported a slight up-regulation of some proteasome genes by chemical or genetic Nrf2 overexpression (54). Starting with an in silico analysis of evolutionally conserved regions in proteasome genes and an algorithms based on Wang's publication of bases restrictions, we identified putative Antioxidant Response Elements in several proteasome subunits. More importantly, we found that some proteasome genes, including PSMB7, were

regulated by Nrf2 because in Nrf2-/- mice baseline levels of expression was slightly lowere. the most interecting observtiosn was that challenging the proteasloem bay a-SYN overexpression lead to incres levesl of a PSM7 in Nrf2+/+ mice but not in Nrf2-/- mice. Accorting to these results the concept fo phase 2 regulated genes by Nrf2 must be expanded to consider the proteasome as part of antioxidant response elicited by Nrf2 and may play a relevant role in protection against a-synucleinopathy.

Gliosis and neuroinflammation are events associated with early PD that can be replicated in the rAAV6-α-SYN model. Here, we report that $Nrf2^{-/-}$ mice presented exhacerbared gliosis and pro-inflammatory manifestations in response to α-SYN. We found that both $Nrf2^{+/+}$ and $Nrf2^{-/-}$ astrocytes took α-SYN a process resembling astrocyte α-synucleinopathy reported in sporadic PD (55) and diffuse Lewy body disease (56). Astrocytes from both genotypes increased expression of pro-inflammatory genes encoding for IL-6, IL-1β and iNOS. This essentially similar response in the two genotypes was consistent with the lack of phase 2 induction, suggesting that in this cell type α-SYN does not provoke a gross release of ROS and does not activate the Nrf2 response. This observation appears to be different from the observed induction of HO-1 in post-mortem PD brains (Fig. 10). We speculate that induction of the phase 2 response in the astrocytes is not a direct consequence of α-SYN signaling but most likely results from interaction with other molecules released to the brain parenchyma.

The effect of α-SYN on microglial cultures was more noticeable than on astrocytes. Here, α-SYN enhanced microglial phagocytosis in $Nrf2^{+/+}$ animals, in agreement with Park et al. (57) but phagocytosis in $Nrf2^{-/-}$ microglia was significantly reduced as determined by counting endocytosis of fluorescent beads. These results indicated that Nrf2 is also involved in the phagocytic process in concordance with the findings that macrophages from $Nrf2^{-/-}$ mice showed lower phagocytosis index (58). But

more importantly, we describe for the first time that, two of the three TAM receptors, Mer and Axl, were significantly down-regulated in $Nrf2^{-/-}$ mice, although only Axl exhibited altered response under α-SYN stimulation. The TAM family of receptor protein tyrosine kinases plays a pivotal role in phagocytosis. Particularly Mer, has been shown to be involved in clearance of the apoptotic cells by peripheral macrophages and dentritic cells (59). Although different cell types appear to require different combinations of TAM receptors, regarding microglia it has been described that Gas6 (Growth arrest specific gene 6) induces Axl/Mer family to stimulate phagocytosis and repress transcriptional expression of pro-inflammatory cytokines, including iNOS and IL-1β (45). Therefore our results uncover an unexplored mechanism by which Nrf2 participates in modulation of microglial activation, disfavoring classical pro-inflammatory and supporting alternative pro-phagocytic phenotypes.

In $Nrf2^{+/+}$ but not in $Nrf2^{-/-}$ microglia α-SYN stimulated the expression of phase 2 genes such as those coding HO-1 and NQO1, indicating a novel mechanism pathway activated by α-SYN. Moreover, in $Nrf2^{-/-}$ microglia α-SYN exacerbated a pro-inflammatory response as demonstrated by increased expression of IL-6, IL-1β and iNOS. These results indicate a role for Nrf2 in down-modulation of microglial pro-inflammatory phenotype. To get more insight into the mechanistic connection we used the microglial cell line BV-2. Here, α-SYN induced both the NF-κB pro-inflammatory and Nrf2 anti-inflammatory responses but with different kinetics. Thus, while the protein levels of p65- NF-κB increased within 30 min, Nrf2 induction was delayed to about 2-3 h. Regarding gene expression, iNOS protein levels were increased at 4 h while HO-1 protein levels required 8 h. These different kinetics suggest that NF-κB activation is an early and direct event of α-SYN signaling, while Nrf2 is a secondary event that participates in a later negative loop regulation of NF-κB. We speculate that at

the same time that α-SYN activates the NF-κB signaling pathway, it induces assembling and up-regulation of NADPH oxidase, therefore promoting oxidative stress on the surrounding environment and in the microglia itself. Activation of NADPH oxidase would trigger a second wave of events that would lead to Nrf2 activation. Consistent with our hypothesis, it has been reported that α-SYN induces ROS production in microglia by NADPH oxidase activation which was linked to direct induction of macrophage antigen-1 (Mac-1) receptor (7, 60).

To determine the relevance of Nrf2 and phase 2 genes in the human PD pathology, we analyzed HO-1 expression in postmortem biopsies of patients in a middle stage of PD progression. The immunodetection specificity was previously demonstrated by lack of signal staining in brain of HO-1-knockout mice (47). In control asymptomatic subjects, HO-1 expression was below the level of detection. However, in PD patients we observed a weak staining in DAergic neurons and astrocytes in agreement with a previous report (61), but not decorating Lewy bodies. More importantly for this study, we show for the first time that clusters of microglial cells are HO-$1^{+}$ in PD patients in areas close to dystrophic dopaminergic neurons. The increase in HO-1 staining observed in these cell types suggests the presence of exacerbated oxidative and inflammatory stress. At the same time, the fact that phase 2 induction was not generalized among all cells in SN, either neurons, astrocytes or microglia, suggests that induction of the phase 2 defense was not sufficient to elicit an efficient protection. These results are consistent with reports indicating that Nrf2 activity declines with age (62, 63), which is the main risk factor for PD.

Several hallmarks of PD such as mitochondrial generation of oxidative stress, association with environmental toxins, proteinopathy and early inflammation are all targeted by Nrf2 through control of redox homeostasis, biotransformation, proteasome

regulation and inhibition of NF-kB, respectively. However, because Nrf2 has a tremendous impact on many aspects of cell and tissue homeostasis it may be anticipated that its effects are not specific for α-SYN-induced neuron damage, gliosis and inflammation. In this regard, Nrf2 might fall in the category of defensive transcription factors, such as HIF in hypoxia or ATF-4 in unfolded protein response, which participate in cell and tissue damage control. Therefore, the activation of Nrf2 should not necessarily provide a therapeutic benefit exclusively for PD but also for other diseases that show signs of oxidative stress and low-grade chronic inflammation such as Alzheimer's disease or Huntington's disease. At the same time, because of its relatively unspecific impact on brain protection, targeting Nrf2 might also contribute to amelioration of non-motor symptoms of PD by protecting non-dopaminergic pathways.

## MATERIALS AND METHODS

*Animals and treatments*

Colonies of Nrf2 knockout ($Nrf2^{-/-}$) mice as well as wild type ($Nrf2^{+/+}$) littermates were established from funders provided by Dr. Masayuki Yamamoto (Tohoku University Graduate School of Medicine, Sendai, Japan) (64). All animal protocols were approved by the Ethical Committee for Research of the *Universidad Autónoma de Madrid* following institutional, Spanish and European guidelines (*Boletín Oficial del Estado* (BOE) of 18 March 1988; and 86/609/EEC, 2003/65/EC European Council Directives).

*Production of the viral vectors and surgical procedures.*

Transfer plasmids for pseudotyped rAAV6 vector production were prepared by cloning a human synapsin 1 promoter driving GFP or α-SYN into pTR-UF20 plasmid. Woodchuck hepatitis virus post-translational regulatory element (WPRE) and poly A signal were inserted downstream to the gene of interest. The protocol for viral vector production was previously described (15). Both GFP and α-SYN vector batches yielded 4.0E13 genome copy/ml titers. The stock preparations were diluted 10 fold for *in vivo* injections. Viral vector injections were performed under ketamine/xylazine anesthesia (8 mg/kg ketamine and 1.2 mg/kg xylazine) of adult mice weighing 20-25 g. Surgery was performed using a stereotaxic frame (Stoelting, Wood Dale, IL, USA) and a 5 µl Hamilton syringe fitted with a pulled glass capillary (outer diameter of 60–80 µm). Animals received a single 2 µl injection into the right SN at the following coordinates: -2.5 mm posterior and -1.4 mm lateral to bregma, and -4.5 mm ventral relative to dura, calculated according to the mouse atlas of Franklin and Paxinos (Franklin and Paxinos, 2008). Vector stocks were injected at a rate of 0.4 µl ⁄ min and the needle was left in

position for an additional 5 min after the infusion was completed before being slowly retracted. Animals were then sutured and returned to their cage.

*HPLC determination of DA and DA metabolites*

The tissue content of dopamine (DA) and 3,4-dihydroxyphenylacetic acid (DOPAC) were assessed through HPLC. After decapitation, the brains were rapidly removed, and the striatum were dissected out. The dissected tissue was rapidly frozen on dry ice and kept at −80 °C until further processing. At the time of analysis, tissue samples were homogenized in 0.1 M perchloric acid and centrifuged at 10,000 rpm for 10 min before being filtered through a PVDF filter (0.45μm; Uni-filter) and spun down for an additional 3 min at 10,000 rpm. 10 μL of the final filtrate of each sample was injected by a cooled Alexys AS 100 autosampler into Alexys Monoamine Analyzer (Antec Leyden, Netherlands) consisting of a DECADE II electrochemical detector and VT-3 electrochemical flow cell. The mobile phase (50 mM phosphoric acid, 50 mM citric acid, 8 mM NaCl, 0.1 mM EDTA, 12.5 % methanol, 600 mg/L octane sulfate; pH 3.1) passed through a 1mm × 150mm column with 3-μm particle size (ALF-115) (Antec Leyden, Netherlands) at a flow rate of 100 μL/min for determination of DA and DOPAC.

*Immunohistochemistry of mouse and human tissues*

Animals were anesthetized with 8 mg/kg ketamine and 1.2 mg/kg xylazine i.p. and then perfused with 4% paraformaldehyde (PFA) dissolved in phosphate buffer pH 7.4. Then, brains were dissected and immersed overnight in the same fixative. Coronal brain sections (30 μm) were obtained on a freezing microtome (Hyrax S 50, Madrid, Spain) and kept in anti-freezing solution at -20ºC until use. Immunostaining was carried

out on free-floating sections with a standard avidin-biotin immunohistochemical protocol previously described (24). The sections were incubated with specific primary antisera (Ab-I), a rabbit tyrosine hydroxylase antiserum (TH) (Chemicon Int., Temecula, CA) diluted 1:1.000; mouse anti α-SYN (BD Bioscience) diluted 1:1.000 and mouse anti green fluorescent protein (GFP) (Sigma Aldrich, St. Louis, USA) diluted 1:1000, in PBST solutions containing normal goat serum. After careful washing, the sections were incubated with the secondary biotinylated secondary antisera (Vector Labs Inc, Burlingame, CA) at room temperature and developed using diaminobenzidine (DAB).

Postmortem brain tissues were obtained from one control (age 58 years) and four PD patients (age range 62–75 years) within a 12 h postmortem interval, according to the standardized procedures of Banco de Tejidos de la Fundación CIEN (Madrid, Spain). The control subject had no background of neuropsychiatric disease and a full neuropathological examination on paraffin-embedded tissue excluded relevant brain pathology. PD diagnosis was confirmed by haematoxylin & eosin and α-SYN staining on paraffin-embedded tissue sections from the same cases used in the immunohistochemical studies. All PDs were categorized within Braak stages 4-5 for Lewy body pathology progression (1).

After paraffin embedding, mesencephalon consecutive sections of 4 µm were stained with antibodies for tyrosine hydroxylase (TH) and heme oxygenase (HO-1), α-SYN and HO-1, GFAP and HO-1, Iba-1 and HO-1. To obtain a more efficient immunostaining, tissue sections were subjected to different antigen retrieval procedures, depending on the antibody requirement. Primary antibody were incubated with Dako REAL antibody diluents (Dako Diagnostics, Spain) for 1 h at RT; TH (1:200, clone LNC1), α-synuclein (1:2000), GFAP (1:1000) and HO-1 (1:200) all from Millipore

Iberica, Spain; and Iba-1 (1:500, Wako Chemicals, Neuss, Germany). After washing, the sections were incubated with the secondary biotinylated antisera (Vector) at room temperature and then with the ABC kit system, and developed using DAB. In the case of HO-1 immunohistochemistry, the secondary antibody was EnVision+ System-HRP (Dako Diagnostics). The images were captured using Axiophot microscope (Carl Zeiss MicroImaging, LLC, United States) at 20X or 40X.

*Stereological analysis*

The total number of $TH^+$ neurons in the SN were estimated using an unbiased stereological quantification method by employing the optical fractionator principle (65, 66) in the light microscopy facility at the DZNE. All quantifications were done after blinding the identity of the sections by a coding system and then excluding the samples that had lower than 60% transgene transduction in the SN. For the analysis every forth section throughout SN was used and the borders for the region of interest were defined by using a 4x objective. Cell counting was performed as previously described by (15). Coefficient of error attributable to the sampling was calculated according to Gundersen and Jensen (67), and values $\leq 0.10$ were accepted.

*Immunofluorescence*

Sections were rinsed in TBS and the protocol followed was previously described by Rojo et al. (24). The sections were incubated 24 h at RT in the following primary antibodies: rabbit anti-Iba1 (1:100, Wako Chemicals), rabbit anti-GFAP (1:500, Dako Diagnostics), mouse anti α-SYN (1:1000, BD Bioscience), mouse anti-TH (1:250, Chemicon International, Inc.), rabbit anti-synaptophysin (1:250, Synaptic Systems GmbH), rabbit anti- α-SYN (phospho S129) (1:150, Abcam, Cambridge, UK), mouse

anti-beta 2 subunit, 20S proteasoma (PSMB7) (1:500, Enzo Life Sciences) and mouse anti-GFP (1:1.000, Sigma Aldrich). Sections were rinsed in TBS and washed three times and then incubated with secondary antibodies for 45 min: Alexa Fluor 546 goat anti-mouse, Alexa 546 goat anti-rabbit or Alexa Fluor 488 goat anti-mouse at a 1:500 dilution (Invitrogen), respectively. Control sections were run following identical protocols but omitting the primary antibody. The fluorescence images were captured using appropriate filters in a Leica DMIRE2TCS SP2 confocal microscope (Nussloch, Germany). The lasers used were Ar 488 nm for green fluorescence and Ar/HeNe 543 nm for red fluorescence and Ar 351 nm and 364 nm for UV fluorescence.

*Cell culture*

For primary mouse microglial and astroglial cell cultures, mixed glial cultures were established. Neonatal (P0-P2) mouse cortex from $Nrf2^{+/+}$ and $Nrf2^{-/-}$ were mechanically dissociated and the cells were seeded onto 75 $cm^2$ flasks in DMEM, supplemented with 10% FCS and penicillin/streptomycin. Cells were cultured in a humidified atmosphere of 5% $CO_2$ at 37°C and the medium was changed the day after seeding and once a week thereafter. Following 2 weeks in culture, flasks were trypsinized and separated using CD11b MicroBeads for magnetic cell sorting (MACS Miltenyi Biotec, Germany), cells were pelleted separately and seeded onto plates in medium. The cultures were at least 99% pure, as judged by immunocytochemical criteria. 24 hours before treatment, medium was changed to DMEM serum-free without antibiotics. Microglia and astrocytes were treated with 1 μM α-SYN (Sigma-Aldrich, Spain) for 4 and 8 h, respectively. α-SYN was aged in PBS at 37ºC for 7 days to obtain oligomeric α-SYN, which was used at a final concentration of 1 μM.

BV2 microglial cells were cultured in RPMI 1640 medium supplemented with 10% FCS and 80 µg/ml gentamicin in a humidified atmosphere of 5% $CO_2$ at 37°C with medium changed every 3–4 days. 24h before the experiments, medium was changed to RPMI serum-free without antibiotics. Cells were treated with 1 µM α-SYN for 4 and 8 h, respectively.

Embryonic skin fibroblasts from mice (MEFs) from $Nrf2^{+/+}$ and $Nrf2^{-/-}$ mice were isolated around embryonal day 13.5. Skin pieces were minced in 3 cm Petri dishes and underwent enzymatic digestion at 37°C for 30 min in Falcon tubes with 1 ml HyQTase (Hyclone, Fisher Scientific España). The digested tissue was passed through a 160 µm Nitex filter into 3 cm Petri dishes, and the enzymes neutralised with DMEM + 15% bovine growth serum (Hyclone). The resulting suspension was centrifuged at 450 × g for 5 min, and the cells were plated at a density of $1 \times 10^6$ cells/$cm^2$ in culture flasks. The fibroblasts were placed in an incubator at 37º C supplemented with 5% $CO_2$, and medium was changed daily for the first three days.

*Human brain extracts*

Forzen postmortem brain tissues were obtained from two control (age 58 and ??? years) and three PD patients (age range 73–85 years) within a 5 h postmortem interval, according to the standardized procedures of Banco de Tejidos de la Fundación CIEN (Madrid, Spain). SN lysates were prepared in RIPA-Buffer (25 mM Tris-HCl pH 7.6, 150 mM NaCl, 1 mM EGTA, 1% Igepal, 1% sodium deoxycholate, 0.1 % SDS, 1 mM PSMF, 1 mM $Na_3VO_4$, 1 mM NaF, 1 µg/ml aprotinin, 1 µg/ml leupeptin and 1 µg/ml pepstatin). 50 µg of protein were loaded for SDS-PAGE electrophoresis.

*Immunoblotting*

The primary antibodies used were anti-p65 (1:2000, Calbiochem, Merck Chemicals International), anti-Nrf2 (1:2000, generous gift of Dr. John Hayes, Biomedical Research Institute, Ninewells Hospital and Medical School,University of Dundee, Scotland, United Kingdom), anti-HO1 (1:1000, Millipore Iberica), anti-iNOS and anti-Iba1 (1:1000, Abcam, Cambridge, UK), anti-GFAP (1:10.000, Sigma-Aldrich) and anti-β-actin (1:2000, Santa Cruz Biotechnology, Santa Cruz, CA). Cell lysates were resolved in SDS-PAGE and transferred to Immobilon-P membranes (Millipore Iberica). These membranes were analyzed using the primary antibodies indicated above and appropriate peroxidase-conjugated secondary antibodies. Proteins were detected by enhanced chemiluminescence (Amersham).

*Proteasome activity assays*

Proteasome activity was assessed in MEFs extracts using fluorogenic peptides. Briefly, cells were sonicated in ice-cold buffer (50 mM Hepes pH 7.54, 150 mM NaCl, 5 mM EDTA, 0.1 mM leupeptin, 1 μg/ml pepstatin A and 1 mM PSMF) and extracts prepared by centrifugation for 15 min at 3,000g. Proteasome-specific peptidase activities were assayed by monitoring the production of 7-amino-4-methylcoumarin (AMC) from the following fluorogenic peptides (Bachem, CH): 100 μM Suc-LLVY-AMC (for chymotrypsin-like), 100 μM Boc-LLR-AMC (for trypsin-like) and 100 μM Z-LLE-AMC (for PGPH or caspase-like activity) in 20 mM Hepes pH 7.4. Reactions were started by adding an aliquot of cellular extract and the fluorescence of released AMC (excitation, 380 nm; emission, 460 nm) was monitored continuously at 37°C in a standard microtiter plate fluorometer (*Synergy*™ HT, Bio-Tek Instruments. GmbH, Friedrichshall, Germany). Background activity (caused by nonproteasomal degradation) was determined by addition of the proteasome inhibitor MG132 at a final concentration

of 100 μM. Assays were calibrated using standard solutions of free fluorophores. Substrate consumption at the end of incubation never exceeded 1%.

*Immunocytochemistry*

Astrocytes and microglia were seeded in 24-well plates. After 24 h cells were shifted to serum-free medium without antibiotics. After treatment with 1 μM α-SYN for 8h, cells were washed with cold PBS and fixed with 4% PFA for 10 min. Cells were permeabilized with 0.25% Nonidet P-40 (Sigma-Aldrich) for 10 min and incubated with primary antibodies for 1.5 h at 37°C in a humidified box. Secondary antibodies were incubated for 45 min at 37°C in the same conditions. To visualize the nuclei, cells were stained with 4′,6′-diamino-2-phenylindole (Molecular Probes, Leiden, The Netherlands). Fluorescent images were captured using appropriate filters in a Leica DMIRE2TCS SP2 confocal microscope (Leica, Nussloch, Germany). Primary antibodies used in immunocytochemistry were rabbit anti-GFAP (1:500, Dako, Millipore), rabbit anti-Iba1 (1:100, Wako Chemicals, Neuss, Germany) and anti- α-SYN (1:1000, BD Bioscience). Secondary antibodies were goat anti-mouse Alexa Fluor 488-conjugated IgG and goat anti-rabbit Alexa Fluor 546-conjugated IgG (Molecular Probes).

*Phagocytosis assay*

Microglial cells from $Nrf2^{+/+}$ and $Nrf2^{-/-}$ mice were collected as described above and 150.000 cells were plated in coverslips overnight. The medium was removed and replaced with serum-free DMEM without antibiotics for 24 h before the start of the experiment. Fluorescent microspheres (FluoSpheres polystyrene microspheres, Invitrogen) were added (150 microspheres per cell) and incubated for 2 h. Then, cells

were washed with PBS, fixed with 4% PFA, and stained with DAPI. The images were captured using 90i Nikon microscope (Nikon, Montreal, QC, Canada) at 40X.

*Analysis of mRNA levels by quantitative real-time PCR*

Total RNA from microglial and astroglial primary cultures and BV2 cells was extracted using TRIzol reagent according to the manufacturer´s instructions (Invitrogen). One microgram of RNA from the different treatments were treated with DNase (Invitrogen) and reverse-transcribed using 4 µl of High capacity RNA-to-cDNA Master Mix (Applied Biosystem, Foster City, CA). For Real-Time PCR analysis we performed the method previously described by Rojo et al (24). Primer sequences are shown in Table 1. To ensure that equal amounts of cDNA were added to the PCR, the β-actin housekeeping gene was amplified. Data analysis is based on the ΔΔCt method with normalization of the raw data to housekeeping genes as described in the manusfacturer´s manual (Applied Biosystem). All PCRs were performed in triplicates.

*Statistical analyses*

Data are presented as mean ± SEM. One and two-way analysis of variance with *post hoc* Newman-Keuls test and Bonferroni's test respectively were used, as appropriate. A Student's *t* test was used to assess differences between groups.

**ACKNOWLEDGMENTS**

This work was supported by grants SAF2010-172218 to AC from the Spanish MICINN, “Bolsa de Investigación L’Oreal-UNESCO 2010” to ILB, Swedish Research Council (K2009-61-20945-03-1), European Community's Seventh Framework Programme FP7-HEALTH-2009 under grant agreement no. 241791 (MEFOPA), and from the European Research Council under grant agreement no. ERC-2009-StG 242932 (TreatPD) to DK. ILB is recipient of a Ramón y Cajal contract (MICINN-RYC) and AU is a recipient of European Union Marie Curie Actions Research Training Network Program in Nervous System Repair (MRTN-CT-2003-504636). We also thank Rosa Ana Ramírez, Johanna Troya Balseca, Ana Belén Rebolledo, Hongyan Liu and Ulla Samuelsson for their technical support.

## REFERENCES


1 Braak, H., Del Tredici, K., Rub, U., de Vos, R.A., Jansen Steur, E.N. and Braak, E. (2003) Staging of brain pathology related to sporadic Parkinson's disease. *Neurobiol Aging*, **24**, 197-211.

2 Lees, A.J., Hardy, J. and Revesz, T. (2009) Parkinson's disease. *Lancet*, **373**, 2055-2066.

3 Hardy, J. (2010) Genetic analysis of pathways to Parkinson disease. *Neuron*, **68**, 201-206.

4 Lotharius, J. and Brundin, P. (2002) Impaired dopamine storage resulting from alpha-synuclein mutations may contribute to the pathogenesis of Parkinson's disease. *Hum Mol Genet*, **11**, 2395-2407.

5 Outeiro, T.F., Klucken, J., Bercury, K., Tetzlaff, J., Putcha, P., Oliveira, L.M., Quintas, A., McLean, P.J. and Hyman, B.T. (2009) Dopamine-induced conformational changes in alpha-synuclein. *PLoS One*, **4**, e6906.

6 Bisaglia, M., Tosatto, L., Munari, F., Tessari, I., de Laureto, P.P., Mammi, S. and Bubacco, L. (2010) Dopamine quinones interact with alpha-synuclein to form unstructured adducts. *Biochem Biophys Res Commun*, **394**, 424-428.

7 Zhang, W., Wang, T., Pei, Z., Miller, D.S., Wu, X., Block, M.L., Wilson, B., Zhou, Y., Hong, J.S. and Zhang, J. (2005) Aggregated alpha-synuclein activates microglia: a process leading to disease progression in Parkinson's disease. *FASEB J*, **19**, 533-542.

8 Lee, J.K., Tran, T. and Tansey, M.G. (2009) Neuroinflammation in Parkinson's disease. *J Neuroimmune Pharmacol*, **4**, 419-429.

9 Halliday, G.M. and Stevens, C.H. (2011) Glia: initiators and progressors of pathology in Parkinson's disease. *Mov Disord*, **26**, 6-17.

10 Austin, S.A., Floden, A.M., Murphy, E.J. and Combs, C.K. (2006) Alpha-synuclein expression modulates microglial activation phenotype. *J Neurosci*, **26**, 10558-10563.

11 Meredith, G.E., Sonsalla, P.K. and Chesselet, M.F. (2008) Animal models of Parkinson's disease progression. *Acta Neuropathol*, **115**, 385-398.

12 Eslamboli, A. (2005) Assessment of GDNF in primate models of Parkinson's disease: comparison with human studies. *Rev Neurosci*, **16**, 303-310.

13 Georgievska, B., Kirik, D., Rosenblad, C., Lundberg, C. and Bjorklund, A. (2002) Neuroprotection in the rat Parkinson model by intrastriatal GDNF gene transfer using a lentiviral vector. *Neuroreport*, **13**, 75-82.

14 Kirik, D., Georgievska, B., Rosenblad, C. and Bjorklund, A. (2001) Delayed infusion of GDNF promotes recovery of motor function in the partial lesion model of Parkinson's disease. *Eur J Neurosci*, **13**, 1589-1599.

15 Decressac, M., Ulusoy, A., Mattsson, B., Georgievska, B., Romero-Ramos, M., Kirik, D. and Bjorklund, A. (2011) GDNF fails to exert neuroprotection in a rat {alpha}-synuclein model of Parkinson's disease. *Brain*.

16 Lo Bianco, C., Deglon, N., Pralong, W. and Aebischer, P. (2004) Lentiviral nigral delivery of GDNF does not prevent neurodegeneration in a genetic rat model of Parkinson's disease. *Neurobiol Dis*, **17**, 283-289.

17 Kirik, D., Georgievska, B., Burger, C., Winkler, C., Muzyczka, N., Mandel, R.J. and Bjorklund, A. (2002) Reversal of motor impairments in parkinsonian rats by

continuous intrastriatal delivery of L-dopa using rAAV-mediated gene transfer. *Proc Natl Acad Sci U S A*, **99**, 4708-4713.
18 Ulusoy, A., Decressac, M., Kirik, D. and Bjorklund, A. (2010) Viral vector-mediated overexpression of alpha-synuclein as a progressive model of Parkinson's disease. *Prog Brain Res*, **184**, 89-111.
19 Kirik, D., Annett, L.E., Burger, C., Muzyczka, N., Mandel, R.J. and Bjorklund, A. (2003) Nigrostriatal alpha-synucleinopathy induced by viral vector-mediated overexpression of human alpha-synuclein: a new primate model of Parkinson's disease. *Proc Natl Acad Sci U S A*, **100**, 2884-2889.
20 Braak, H. and Braak, E. (2000) Pathoanatomy of Parkinson's disease. *J Neurol*, **247 Suppl 2**, II3-10.
21 Galvin, J.E., Uryu, K., Lee, V.M. and Trojanowski, J.Q. (1999) Axon pathology in Parkinson's disease and Lewy body dementia hippocampus contains alpha-, beta-, and gamma-synuclein. *Proc Natl Acad Sci U S A*, **96**, 13450-13455.
22 St Martin, J.L., Klucken, J., Outeiro, T.F., Nguyen, P., Keller-McGandy, C., Cantuti-Castelvetri, I., Grammatopoulos, T.N., Standaert, D.G., Hyman, B.T. and McLean, P.J. (2007) Dopaminergic neuron loss and up-regulation of chaperone protein mRNA induced by targeted over-expression of alpha-synuclein in mouse substantia nigra. *J Neurochem*, **100**, 1449-1457.
23 Innamorato, N.G., Rojo, A.I., Garcia-Yague, A.J., Yamamoto, M., de Ceballos, M.L. and Cuadrado, A. (2008) The transcription factor Nrf2 is a therapeutic target against brain inflammation. *J Immunol*, **181**, 680-689.
24 Rojo, A.I., Innamorato, N.G., Martin-Moreno, A.M., De Ceballos, M.L., Yamamoto, M. and Cuadrado, A. (2010) Nrf2 regulates microglial dynamics and neuroinflammation in experimental Parkinson's disease. *Glia*, **58**, 588-598.
25 Jazwa, A., Rojo, A.I., Innamorato, N.G., Hesse, M., Fernandez-Ruiz, J. and Cuadrado, A. (2011) Pharmacological Targeting of the Transcription Factor Nrf2 at the Basal Ganglia Provides Disease Modifying Therapy for Experimental Parkinsonism. *Antioxid Redox Signal*.
26 Innamorato, N.G., Lastres-Becker, I. and Cuadrado, A. (2009) Role of microglial redox balance in modulation of neuroinflammation. *Curr Opin Neurol*, **22**, 308-314.
27 Ramsey, C.P., Glass, C.A., Montgomery, M.B., Lindl, K.A., Ritson, G.P., Chia, L.A., Hamilton, R.L., Chu, C.T. and Jordan-Sciutto, K.L. (2007) Expression of Nrf2 in neurodegenerative diseases. *J Neuropathol Exp Neurol*, **66**, 75-85.
28 von Otter, M., Landgren, S., Nilsson, S., Celojevic, D., Bergstrom, P., Hakansson, A., Nissbrandt, H., Drozdzik, M., Bialecka, M., Kurzawski, M. *et al.* (2010) Association of Nrf2-encoding NFE2L2 haplotypes with Parkinson's disease. *BMC Med Genet*, **11**, 36.
29 von Otter, M., Landgren, S., Nilsson, S., Zetterberg, M., Celojevic, D., Bergstrom, P., Minthon, L., Bogdanovic, N., Andreasen, N., Gustafson, D.R. *et al.* (2010) Nrf2-encoding NFE2L2 haplotypes influence disease progression but not risk in Alzheimer's disease and age-related cataract. *Mech Ageing Dev*, **131**, 105-110.
30 Maingay, M., Romero-Ramos, M., Carta, M. and Kirik, D. (2006) Ventral tegmental area dopamine neurons are resistant to human mutant alpha-synuclein overexpression. *Neurobiol Dis*, **23**, 522-532.
31 Kirik, D. and Bjorklund, A. (2003) Modeling CNS neurodegeneration by overexpression of disease-causing proteins using viral vectors. *Trends Neurosci*, **26**, 386-392.

32 Kirik, D., Rosenblad, C., Burger, C., Lundberg, C., Johansen, T.E., Muzyczka, N., Mandel, R.J. and Bjorklund, A. (2002) Parkinson-like neurodegeneration induced by targeted overexpression of alpha-synuclein in the nigrostriatal system. *J Neurosci*, **22**, 2780-2791.
33 Grealish, S., Mattsson, B., Draxler, P. and Bjorklund, A. (2010) Characterisation of behavioural and neurodegenerative changes induced by intranigral 6-hydroxydopamine lesions in a mouse model of Parkinson's disease. *Eur J Neurosci*, **31**, 2266-2278.
34 Lee, J., Zhu, W.M., Stanic, D., Finkelstein, D.I., Horne, M.H., Henderson, J., Lawrence, A.J., O'Connor, L., Tomas, D., Drago, J. *et al.* (2008) Sprouting of dopamine terminals and altered dopamine release and uptake in Parkinsonian dyskinaesia. *Brain*, **131**, 1574-1587.
35 Perovic, M., Mladenovic, A., Rakic, L., Ruzdijic, S. and Kanazir, S. (2005) Increase of GAP-43 in the rat cerebellum following unilateral striatal 6-OHDA lesion. *Synapse*, **56**, 170-174.
36 Yamamoto, N., Sawada, H., Izumi, Y., Kume, T., Katsuki, H., Shimohama, S. and Akaike, A. (2007) Proteasome inhibition induces glutathione synthesis and protects cells from oxidative stress: relevance to Parkinson disease. *J Biol Chem*, **282**, 4364-4372.
37 Ghee, M., Fournier, A. and Mallet, J. (2000) Rat alpha-synuclein interacts with Tat binding protein 1, a component of the 26S proteasomal complex. *J Neurochem*, **75**, 2221-2224.
38 Marx, F.P., Soehn, A.S., Berg, D., Melle, C., Schiesling, C., Lang, M., Kautzmann, S., Strauss, K.M., Franck, T., Engelender, S. *et al.* (2007) The proteasomal subunit S6 ATPase is a novel synphilin-1 interacting protein--implications for Parkinson's disease. *FASEB J*, **21**, 1759-1767.
39 Bukhatwa, S., Zeng, B.Y., Rose, S. and Jenner, P. (2010) A comparison of changes in proteasomal subunit expression in the substantia nigra in Parkinson's disease, multiple system atrophy and progressive supranuclear palsy. *Brain Res*, **1326**, 174-183.
40 Schell, H., Hasegawa, T., Neumann, M. and Kahle, P.J. (2009) Nuclear and neuritic distribution of serine-129 phosphorylated alpha-synuclein in transgenic mice. *Neuroscience*, **160**, 796-804.
41 Chau, K.Y., Ching, H.L., Schapira, A.H. and Cooper, J.M. (2009) Relationship between alpha synuclein phosphorylation, proteasomal inhibition and cell death: relevance to Parkinson's disease pathogenesis. *J Neurochem*, **110**, 1005-1013.
42 Sanchez-Guajardo, V., Febbraro, F., Kirik, D. and Romero-Ramos, M. (2010) Microglia acquire distinct activation profiles depending on the degree of alpha-synuclein neuropathology in a rAAV based model of Parkinson's disease. *PLoS One*, **5**, e8784.
43 Racchetti, G., D'Alessandro, R. and Meldolesi, J. (2011) Astrocyte stellation, a process dependent on Rac1 is sustained by the regulated exocytosis of enlargeosomes. *Glia*.
44 Lee, H.J., Suk, J.E., Patrick, C., Bae, E.J., Cho, J.H., Rho, S., Hwang, D., Masliah, E. and Lee, S.J. (2010) Direct transfer of alpha-synuclein from neuron to astroglia causes inflammatory responses in synucleinopathies. *J Biol Chem*, **285**, 9262-9272.
45 Grommes, C., Lee, C.Y., Wilkinson, B.L., Jiang, Q., Koenigsknecht-Talboo, J.L., Varnum, B. and Landreth, G.E. (2008) Regulation of microglial phagocytosis and inflammatory gene expression by Gas6 acting on the Axl/Mer family of tyrosine kinases. *J Neuroimmune Pharmacol*, **3**, 130-140.

46 Chen, P.C., Vargas, M.R., Pani, A.K., Smeyne, R.J., Johnson, D.A., Kan, Y.W. and Johnson, J.A. (2009) Nrf2-mediated neuroprotection in the MPTP mouse model of Parkinson's disease: Critical role for the astrocyte. *Proc Natl Acad Sci U S A*, **106**, 2933-2938.
47 Innamorato, N.G., Jazwa, A., Rojo, A.I., Garcia, C., Fernandez-Ruiz, J., Grochot-Przeczek, A., Stachurska, A., Jozkowicz, A., Dulak, J. and Cuadrado, A. (2010) Different susceptibility to the Parkinson's toxin MPTP in mice lacking the redox master regulator Nrf2 or its target gene heme oxygenase-1. *PLoS One*, **5**, e11838.
48 Burton, N.C., Kensler, T.W. and Guilarte, T.R. (2006) In vivo modulation of the Parkinsonian phenotype by Nrf2. *Neurotoxicology*, **27**, 1094-1100.
49 McNaught, K.S., Belizaire, R., Isacson, O., Jenner, P. and Olanow, C.W. (2003) Altered proteasomal function in sporadic Parkinson's disease. *Exp Neurol*, **179**, 38-46.
50 Nakamura, A., Kitami, T., Mori, H., Mizuno, Y. and Hattori, N. (2006) Nuclear localization of the 20S proteasome subunit in Parkinson's disease. *Neurosci Lett*, **406**, 43-48.
51 McNaught, K.S., Jnobaptiste, R., Jackson, T. and Jengelley, T.A. (2010) The pattern of neuronal loss and survival may reflect differential expression of proteasome activators in Parkinson's disease. *Synapse*, **64**, 241-250.
52 Hu, R., Xu, C., Shen, G., Jain, M.R., Khor, T.O., Gopalkrishnan, A., Lin, W., Reddy, B., Chan, J.Y. and Kong, A.N. (2006) Identification of Nrf2-regulated genes induced by chemopreventive isothiocyanate PEITC by oligonucleotide microarray. *Life Sci*, **79**, 1944-1955.
53 Hu, R., Xu, C., Shen, G., Jain, M.R., Khor, T.O., Gopalkrishnan, A., Lin, W., Reddy, B., Chan, J.Y. and Kong, A.N. (2006) Gene expression profiles induced by cancer chemopreventive isothiocyanate sulforaphane in the liver of C57BL/6J mice and C57BL/6J/Nrf2 (-/-) mice. *Cancer Lett*, **243**, 170-192.
54 Kwak, M.K., Cho, J.M., Huang, B., Shin, S. and Kensler, T.W. (2007) Role of increased expression of the proteasome in the protective effects of sulforaphane against hydrogen peroxide-mediated cytotoxicity in murine neuroblastoma cells. *Free Radic Biol Med*, **43**, 809-817.
55 Braak, H., Sastre, M. and Del Tredici, K. (2007) Development of alpha-synuclein immunoreactive astrocytes in the forebrain parallels stages of intraneuronal pathology in sporadic Parkinson's disease. *Acta Neuropathol*, **114**, 231-241.
56 Terada, S., Ishizu, H., Yokota, O., Tsuchiya, K., Nakashima, H., Ishihara, T., Fujita, D., Ueda, K., Ikeda, K. and Kuroda, S. (2003) Glial involvement in diffuse Lewy body disease. *Acta Neuropathol*, **105**, 163-169.
57 Park, J.Y., Paik, S.R., Jou, I. and Park, S.M. (2008) Microglial phagocytosis is enhanced by monomeric alpha-synuclein, not aggregated alpha-synuclein: implications for Parkinson's disease. *Glia*, **56**, 1215-1223.
58 Suganuma, H., Fahey, J.W., Bryan, K.E., Healy, Z.R. and Talalay, P. (2011) Stimulation of phagocytosis by sulforaphane. *Biochem Biophys Res Commun*, **405**, 146-151.
59 Binder, M.D. and Kilpatrick, T.J. (2009) TAM receptor signalling and demyelination. *Neurosignals*, **17**, 277-287.
60 Zhang, W., Dallas, S., Zhang, D., Guo, J.P., Pang, H., Wilson, B., Miller, D.S., Chen, B., McGeer, P.L., Hong, J.S. *et al.* (2007) Microglial PHOX and Mac-1 are essential to the enhanced dopaminergic neurodegeneration elicited by A30P and A53T mutant alpha-synuclein. *Glia*, **55**, 1178-1188.
61 Schipper, H.M., Liberman, A. and Stopa, E.G. (1998) Neural heme oxygenase-1 expression in idiopathic Parkinson's disease. *Exp Neurol*, **150**, 60-68.

62 Sykiotis, G.P. and Bohmann, D. (2010) Stress-activated cap'n'collar transcription factors in aging and human disease. *Sci Signal*, **3**, re3.
63 Suh, J.H., Shenvi, S.V., Dixon, B.M., Liu, H., Jaiswal, A.K., Liu, R.M. and Hagen, T.M. (2004) Decline in transcriptional activity of Nrf2 causes age-related loss of glutathione synthesis, which is reversible with lipoic acid. *Proc Natl Acad Sci U S A*, **101**, 3381-3386.
64 Itoh, K., Chiba, T., Takahashi, S., Ishii, T., Igarashi, K., Katoh, Y., Oyake, T., Hayashi, N., Satoh, K., Hatayama, I. *et al.* (1997) An Nrf2/small Maf heterodimer mediates the induction of phase II detoxifying enzyme genes through antioxidant response elements. *Biochem Biophys Res Commun*, **236**, 313-322.
65 West, M.J., Slomianka, L. and Gundersen, H.J. (1991) Unbiased stereological estimation of the total number of neurons in thesubdivisions of the rat hippocampus using the optical fractionator. *Anat Rec*, **231**, 482-497.
66 Schmitz, C. and Hof, P.R. (2007) Design-Based Stereology in Brain Aging Research.
67 Gundersen, H.J. and Jensen, E.B. (1987) The efficiency of systematic sampling in stereology and its prediction. *J Microsc*, **147**, 229-263.

## FIGURE LEGENDS

**Figure 1**: *Human α-SYN expression at the SN and striatum of Nrf2$^{+/+}$ and Nrf2$^{-/-}$ mice injected with rAAV-α-SYN*. A, Immunohistochemistry for human α-SYN. Midbrain of right side was injected with rAAV-α-SYN expression vector. Left non-injected side is shown as negative control. *Upper panel*, Nrf2$^{+/+}$ mice; *Lower panel*, Nrf2$^{-/-}$ mice. B, Double-immunofluorescence for α-SYN (green) and TH (red) showing colocalization of both antigens in nigral DAergic neurons. C, Immunohistochemistry for human α-SYN at the right striatum of Nrf2$^{+/+}$ mice (*upper panel*) and Nrf2$^{-/-}$ mice (*lower panel*).

**Figure 2**: *Nrf2-deficiency exacerbates TH$^{+}$ neuronal loss induced by α-SYN overexpression at the SN*. Immunohistochemistry for TH$^{+}$ neurons following 8 weeks after injection of rAAV-α-SYN. A, ventral midbrain from Nrf2$^{+/+}$ mice. B, ventral midbrain from Nrf2$^{-/-}$ mice. C and D, high magnification of the right side of SN injected with rAAV-α-SYN in Nrf2$^{+/+}$ and Nrf2$^{-/-}$, respectively. Asterisks indicate regions with loss of TH$^{+}$ neurons; arrows indicate regions with loss of TH$^{+}$ fibers. E-H, Immunohistochemistry for TH at the striatum. E and F, left and right sides in Nrf2$^{+/+}$ mice. G and H, left and right sides in Nrf2$^{-/-}$ mice. I, Stereological counting of nigral TH$^{+}$ neurons (n=3 animals per group). Two-way ANOVA followed by Bonferroni's test was applied to determine the significance of biochemical differences among groups. Asterisk denotes significant differences between treatments with *$p<0.05$. J-L, Neurotransmitter levels measured at the striatum following 8 weeks after rAAV-α-SYN injections. J, DA levels (% of control side); K, DOPAC levels (% of control side); L, DOPAC/DA ratio shown as an estimate of DA catabolism rate (n=5-6 animals per group).

**Figure 3**. *Proteasomal deficiencies in Nrf2$^{-/-}$ mice increased aggregation of α-SYN in neuron bodies and dendrites.* Immunohistochemical detection of dystrophic neurites with α-SYN antibody in Nrf2$^{+/+}$ (A), Nrf2$^{-/-}$ mice (B) and PD patient (C). Arrow heads indicate the presence of dystrophic neuritis both in Nrf2$^{-/-}$ mice and PD patient. Scale bar indicates 20 μm. D, Quantification of the mRNA levels, by qRT-PCR of PSMB7, PSMC3 and PSMC4 (n= 5-6 samples per group). A Student's *t* test was used to assess significant differences among groups and in all cases the p=0.06, nearly statistically significant. Specific mean values $\pm$ SEM were: for PSMB7: Nrf2$^{+/+}$, 1.024 $\pm$ 0.113 and Nrf2$^{-/-}$, 0.830 $\pm$ 0.013; PSMC3: Nrf2$^{+/+}$, 1.012 $\pm$ 0.115 and Nrf2$^{-/-}$, 0.832 $\pm$ 0.015; Nrf2$^{+/+}$, 1.028 $\pm$ 0.120 and Nrf2$^{-/-}$, 0.808 $\pm$ 0.019. E, Photographs show double immunofluorescence staining of 30 μm-thick sections of SN areas from Nrf2$^{+/+}$ and Nrf2$^{-/-}$ injected with rAAV-α-SYN vector with antibodies against α-SYN (green) and PSMB7 (red). Right panels are an amplification of the white squares from the left panels. Scale bars indicate 20 μm.

**Figure 4:** *Enhanced phospho-S129-α-SYN at the SN of Nrf2-/- mice.* Immunofluorescence detection of phospho-S129-α-SYNat the injected side with rAAV6-α-SYN in Nrf2$^{+/+}$ and Nrf2$^{-/-}$ mice. Scale bar indicate 25 μm. Quantification of the fluorescence intensity related to Nrf2$^{+/+}$ mice (n= 4 samples per group). A Student's *t* test was used to assess significant differences among groups. Asterisk denote significant difference *p< 0.05.

**Figure 5**: *Nrf2$^{-/-}$ mice exhibit increased astrogliosis and microgliosis at the SN in the tissue area expressing human α-SYN but not GFP*. Photographs show double immunofluorescence staining of 30 μm-thick sections of SN areas from Nrf2$^{+/+}$ and Nrf2$^{-/-}$ mice following 8 weeks from injection with rAAV-α-SYN or rAAV-GFP vector. A, to analyze astroglia, sections were stained with antibodies against GFAP (red) and

either α-SYN or GFP (both in green). B, quantification of the morphological astrocyte changes. Astrocyte morphology was evaluated as resting (type A) or reactive (typeB). Values were represented as % of total number referred to the ipsilateral side. C, to analyse microglia, sections were stained with antibodies against Iba1 (red) and either α-SYN or GFP (both in green). Scale bars indicate 20 μm. D, quantification of the morphological microglial changes. Microglia morphology was evaluated as resting (type A), initiation of microglial activation (type B), activated but non-phagocytic (type C) and activated phagocytic (type D). Values were represented as % of total number referred to the ipsilateral side.

**Figure 6**: *Effect of human α-SYN on morphology of astrocytes*. A, Primary astrocyte cultures from $Nrf2^{+/+}$ or $Nrf2^{-/-}$ mice were treated with 1μM α-SYN for 8 h. Doble-immunofluorescence analysis was performed using anti-GFAP (green) as astrocyte marker and anti α-SYN (red). Scale bar indicates 15 μm.

**Figure 7:** *Effect of human α-SYN on pro-inflammatory markers of astrocytes.* Quantification of the mRNA levels, measured by qRT-PCR, of HO-1 (A) and NQO1 (B), as well as pro-inflammatoty markers IL-6 (C), IL-1β (D) and iNOS (E) and anti-inflammatory marker IL-4 (F) (n=5 samples per group). One-way ANOVA followed by Newman-Keuls test was used to assess significant differences among groups. Asterisks denote significant differences *$p< 0.05$, **$p<0.01$ comparing the indicated groups.

**Figure 8**: *α-SYN activates NF-κB and Nrf2 pathways in the microglial cell line BV2*. A, immunoblots from microglia submitted to 1μM α-SYN for the indicated times. *Upper panel*, anti-Nrf2 antibody; *middle panel*, anti-p65 NF-κB antibody; lower panel, anti-β-actin antibody showing similar amount of protein per lane. B, quantification of immunoblots from three independent experiments for Nrf2 and p65. C, mRNA levels,

measured by qRT-PCR, for HO-1, IL-1β, IL-6 and iNOS, after 4 and 8 h of exposure to 1μM α-SYN. (n=4 samples per group). One-way ANOVA followed by Newman-Keuls test was used to assess significant differences among groups. Asterisks denote significant differences *p< 0.05, **p<0.01 comparing the indicated groups. D, protein levels for HO-1, iNOS and Iba1 after 4 and 8 h of treatment with 1μM α-SYN. E, quantification of immunoblots for HO-1, iNOS and Iba1. Asterisks denote significant difference *p< 0.05 compared to the basal level.

**Figure 9**: *Effect of human α-SYN on microglial morphology*. Primary microglial cell cultures from $Nrf2^{+/+}$ or $Nrf2^{-/-}$ mice were treated with 1μM α-SYN for 8 h. Double-immunofluorescence analysis was performed using anti-Iba1antibody (green) as microglial marker and anti-α-SYN (red). Scale bar indicates 15 μm.

**Figure 10:** *Effect of human α-SYN on phagocytosis and production of pro-inflammatory markers in microglia.* Quantification of the mRNA levels, by qRT-PCR, of Nrf2 inducible markers HO-1 (A), NQO1 (B) and pro-inflammatory markers IL-6 (C), IL-1β (D) and iNOS (E) (n=4 samples per group). Statistically significant differences are shown with *p< 0.05, **p<0.01 comparing the untreated $Nrf2^{+/+}$ group with the indicated groups or between the indicated groups. F, Effect of α-SYN on the phagocytic response. Microglia from $Nrf2^{+/+}$ or $Nrf2^{-/-}$ mice were incubated with fluorescent microspheres in the absence or presence of 1μM α-SYN for 2 h. Phagocytosis efficiency was calculated as number of microspheres per cell. One-way ANOVA followed by Newman-Keuls test was used to assess significant differences among groups. Asterisks denote significant differences *p< 0.05, **p<0.01, ***p<0.001 comparing the indicated groups. G, H, I, Quantification of mRNA levels by qRT-PCR of the three TAM receptors : Axl (G), Mer (H) and Tyro3 (I) (n= 4-5 samples per group). A Student's *t*

test was used to assess significant differences among groups. Asterisk denotes significant differences *p< 0.05 comparing the indicated groups.

**Figure 11**: *Expression of the phase 2 enzyme HO-1 in microglia and astroglia at the SNpc of PD patients*. Immunohistochemistry of GFAP and HO-1 in two adjacent 4-µm thick sections from in control asymptomatic subject (A) and PD patient with mild degeneration (B). Scale bar indicates 100 µm. C and D, two adjacent 4-µm thick sections from a PD patient stained for HO-1 and GFAP, respectively. The rectangle indicates an astrocyte that in both consecutive sections is doubly labelled for HO-1 and GFAP. Arrows point to the same neuromelanin-containig neuron with a Lewy body. E and F, two adjacent 4-µm thick sections from a PD patient stained for HO-1 and Iba1, respectively. The rectangle indicates microglia that in both consecutive sections is doubly labelled for Iba1 and HO-1. Asterisks show the same neuromelanin-containig neurons in both consecutive sections. Scale bar indicates 50 µm.

**Figure 12:** *SN from PD patients exhibit increased expression of HO-1 correlated with astro- and microgliosis*. Western-blot analysis of HO-1, GFAP and Iba1 in human brain extracts from SN show enhanced protein expression of phase 2 protein HO-1, astrocyte marker GFAP and microglial marker Iba1 in PD patients. The relative optical density of the immunoblot band is also represented (Control n=2; PD n=3). A Student's *t* test was used to assess significant differences among groups. Asterisk denote significant difference *p< 0.05 and **p<0.01.

**Table 1:** Genes and primers used for quantitative PCR amplification

**Supplementary Figure 1**: *Immunoblotting for TH at the striatum*. A, upper panel, TH levels in the striatum from injected (right) versus non-injected side (left) from $Nrf2^{+/+}$ and $Nrf2^{-/-}$ mice with AAV-GFP versus AAV-α-SYN (n=6 per group). The results showed no significant differences between the injected with AAV-α-SYN versus non-injected sides in both genotypes. B, unilateral injection of 1 µl of 6-OHDA (4 µg/µl) into the striatum of $Nrf2^{+/+}$ and $Nrf2^{-/-}$ mice. One month after lesion mice were sacrificed and TH levels were measured in the striatum. In this case we could observe a decreased at the TH levels in the lesioned side which correlated with an increased in GFAP levels.

**Supplementary Figure 2:** *Determination of DAergic axonal sprouting at the striatum after rAAV6 injection in the SN*. Synaptophysin immunofluorescence staining of 30 µm-thick sections of the striatum from $Nrf2^{+/+}$ and $Nrf2^{-/-}$ injected either with rAAV6-GFP or with rAAV6-α-SYN. Scale bars indicate 250 µm. Quantification of the synpatophysin immunoreactivity as particles was performed using Image J. A Student's *t* test was used to assess significant differences among groups. Asterisks denote significant differences **$p<0.01$, ***$p<0.001$ comparing the indicated groups.

**Supplementary Figure 3**: *Control photographs.* Double immunofluorescence staining of 30 µm-thick sections of SN areas from $Nrf2^{+/+}$ and $Nrf2^{-/-}$ injected with rAAV-GFP

vector with antibodies against α-SYN (green) and PSMB7 (red). Scale bars indicate 20 μm.

**Supplementary Figure 4**: *Analysis of the proteasome system in mouse embryonic fribroblast (MEFs) from Nrf2$^{+/+}$ and Nrf2$^{-/-}$ mice*. A, quantification of the mRNA levels in MEFs from Nrf2$^{+/+}$ and Nrf2$^{-/-}$ mice, by qRT-PCR of PSMB7, PSMC3 and PSMC4, at basal levels and after 6h treatment with the proteasome inhibitor MG132 (15 μM) (n=4 samples per group). Two-way ANOVA followed by Bonferroni post-test was used to assess significant differences among groups. Asterisks denote significant differences *p< 0.05, **p<0.01 comparing the indicated groups and ##p<0.01 and ###p<0.001 respect to the basal Nrf2$^{+/+}$ group. B, measurement of the proteasomal enzymatic activities chymiotrypsin, PGPH and trypsin. The absence of Nrf2 leads to the reduction of the chymiotrypsin and PGPH enzymatic activities while trypsin activity remains unchanged.

**Supplementary Figure 5**: *Effect of human oligomeric α-SYN on morphology of astrocytes*. A, Primary astrocyte cultures from Nrf2$^{+/+}$ or Nrf2$^{-/-}$ mice were treated with 1μM oligomeric α-SYN for 8 h. Doble-immunofluorescence analysis was performed using anti-GFAP (green) as astrocyte marker and anti α-SYN (red). Scale bar indicates 15 μm.

**Supplementary Figure 6:** *Effect of human oligomeric α-SYN on microglial morphology*. Primary microglial cell cultures from Nrf2$^{+/+}$ or Nrf2$^{-/-}$ mice were treated

with 1μM oligomeric α-SYN for 8 h. Double-immunofluorescence analysis was performed using anti-Iba1antibody (green) as microglial marker and anti-α-SYN (red). Scale bar indicates 15 μm.

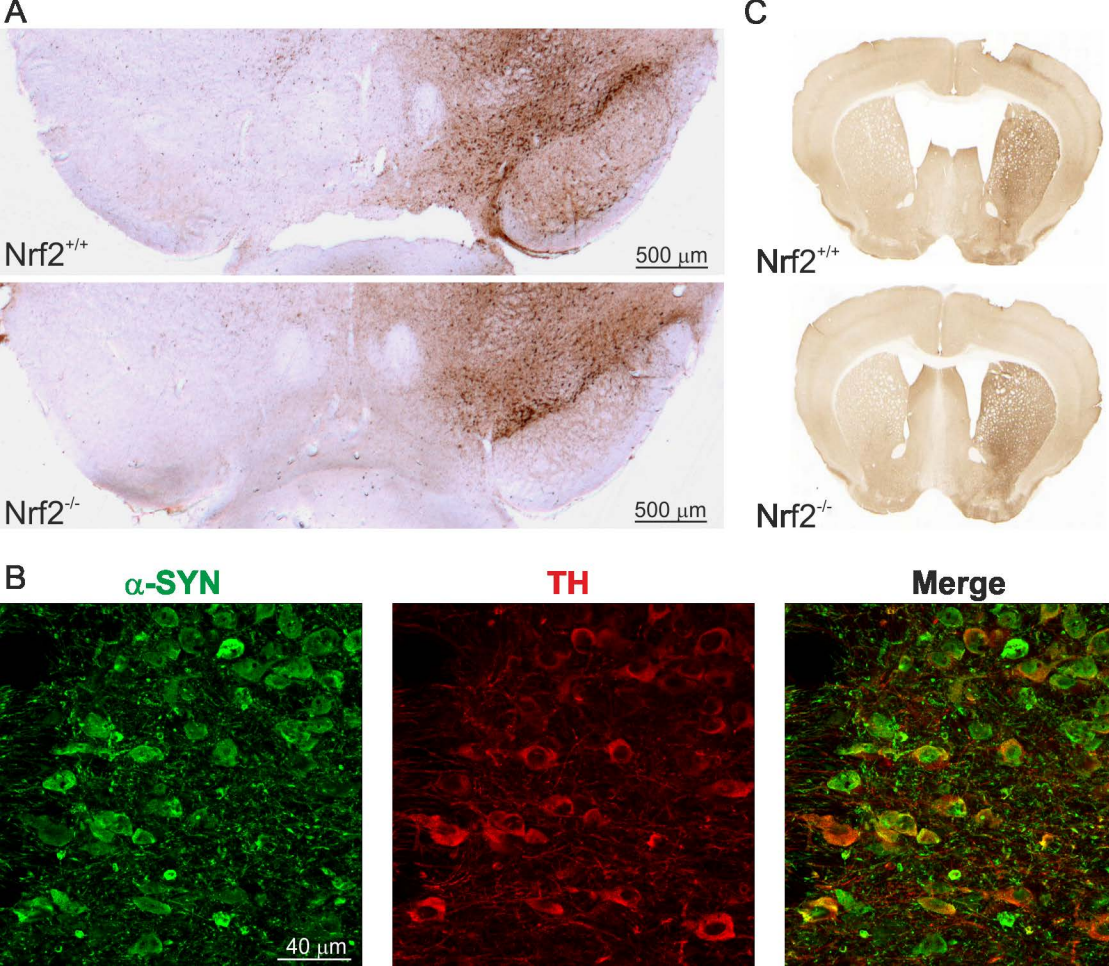
A
Nrf2+/+
500 μm
Nrf2-/-
500 μm
C
Nrf2+/+
Nrf2-/-
B
α-SYN
TH
Merge
40 μm

Figure 2

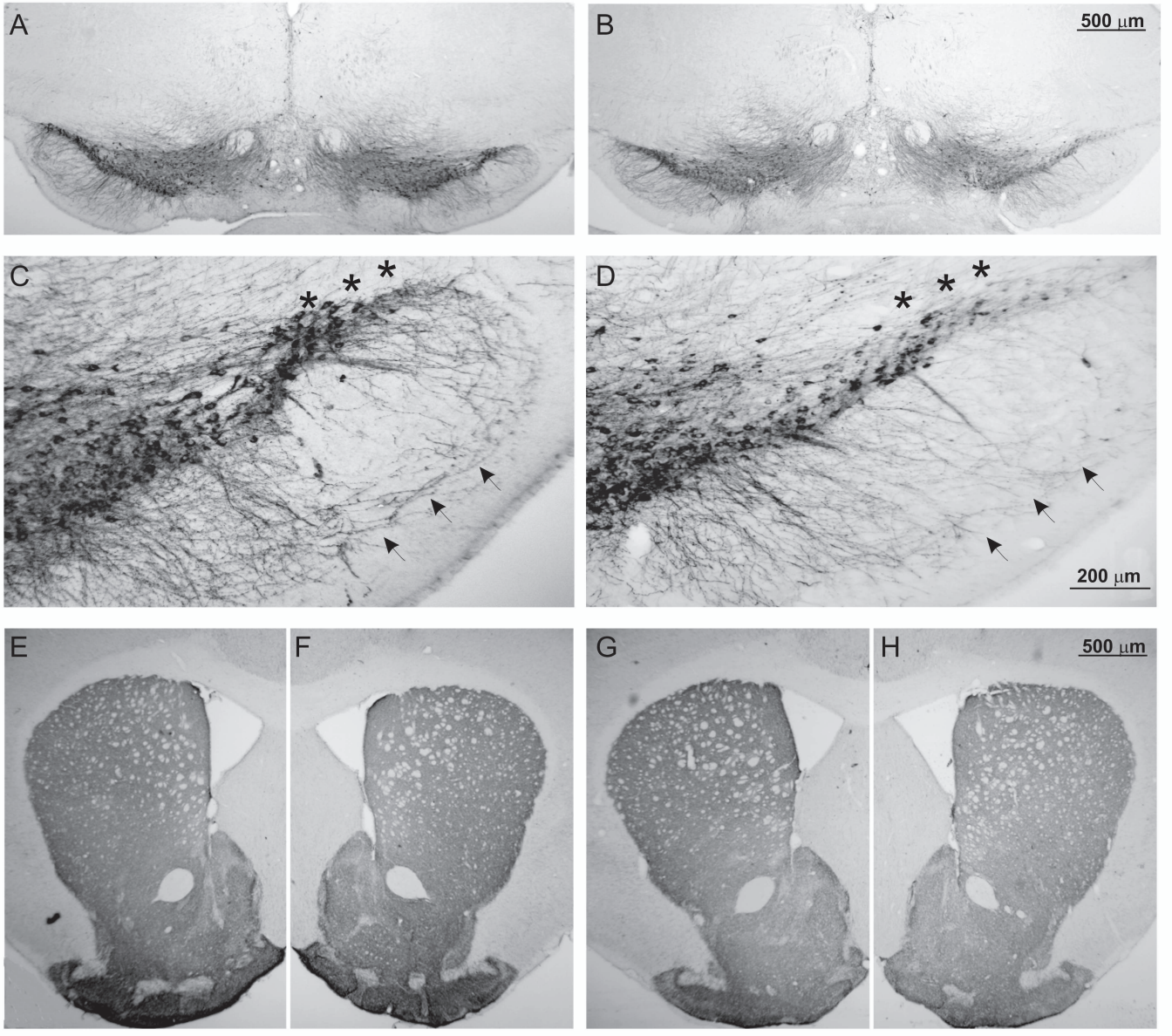
A
B
500 μm
C
D
200 μm
E
F
G
H
500 μm

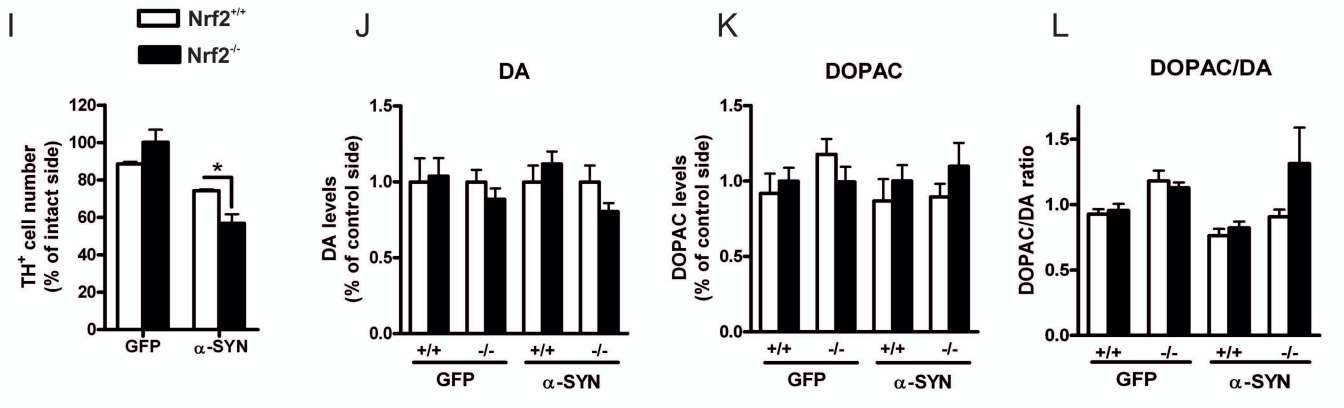
I
Nrf2+/+
Nrf2-/-
TH+ cell number (% of intact side)
120
100
80
60
40
20
0
*
GFP
α-SYN
J
DA
DA levels (% of control side)
1.5
1.0
0.5
0.0
+/+
-/-
+/+
-/-
GFP
α-SYN
K
DOPAC
DOPAC levels (% of control side)
1.5
1.0
0.5
0.0
+/+
-/-
+/+
-/-
GFP
α-SYN
L
DOPAC/DA
DOPAC/DA ratio
1.5
1.0
0.5
0.0
+/+
-/-
+/+
-/-
GFP
α-SYN

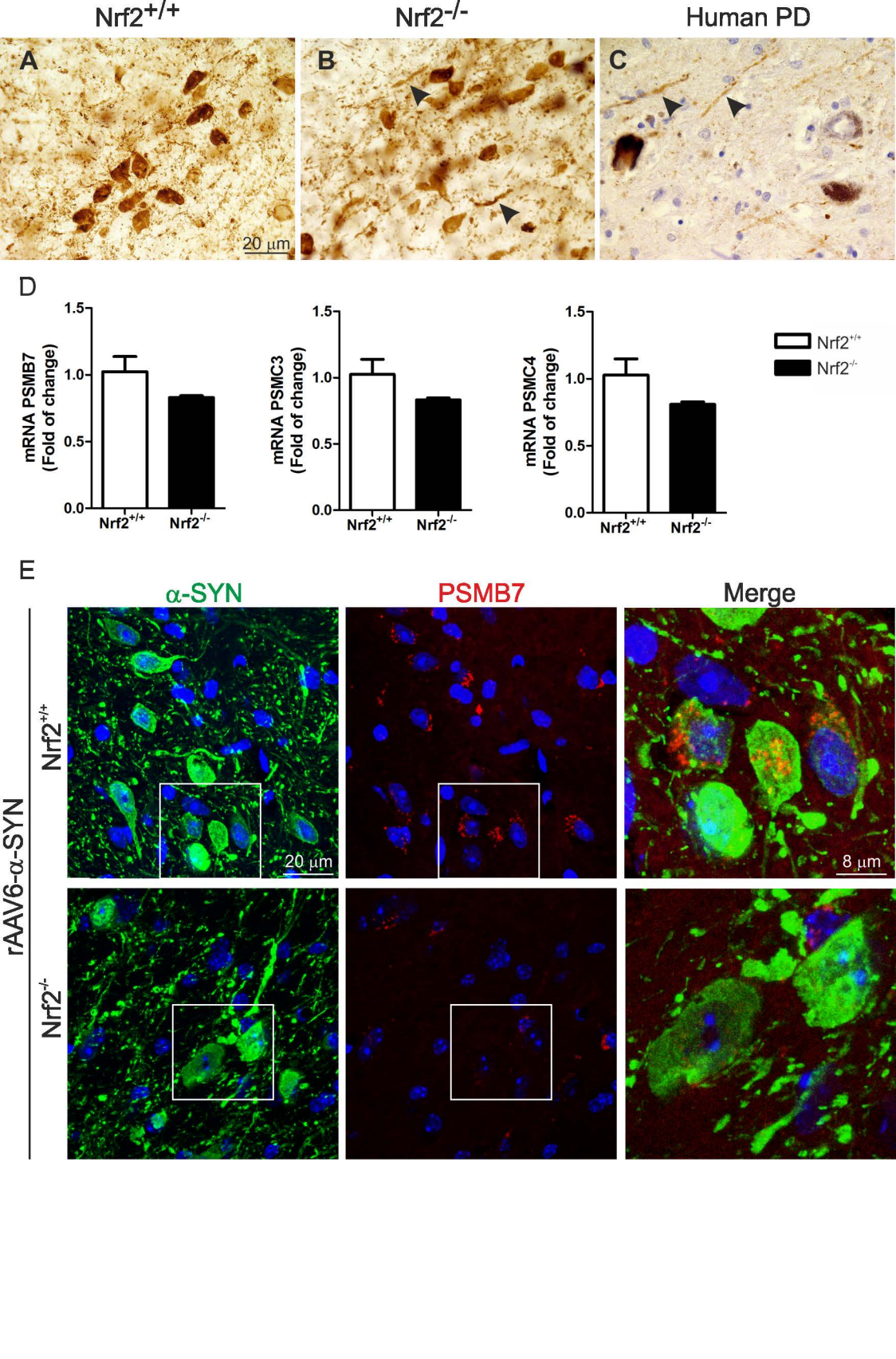
Nrf2+/+
Nrf2-/-
Human PD
A
B
C
20 μm
D
mRNA PSMB7 (Fold of change)
mRNA PSMC3 (Fold of change)
mRNA PSMC4 (Fold of change)
1.5
1.0
0.5
0.0
Nrf2+/+
Nrf2-/-
E
α-SYN
PSMB7
Merge
rAAV6-α-SYN
Nrf2+/+
Nrf2-/-
20 μm
8 μm

Figure 4

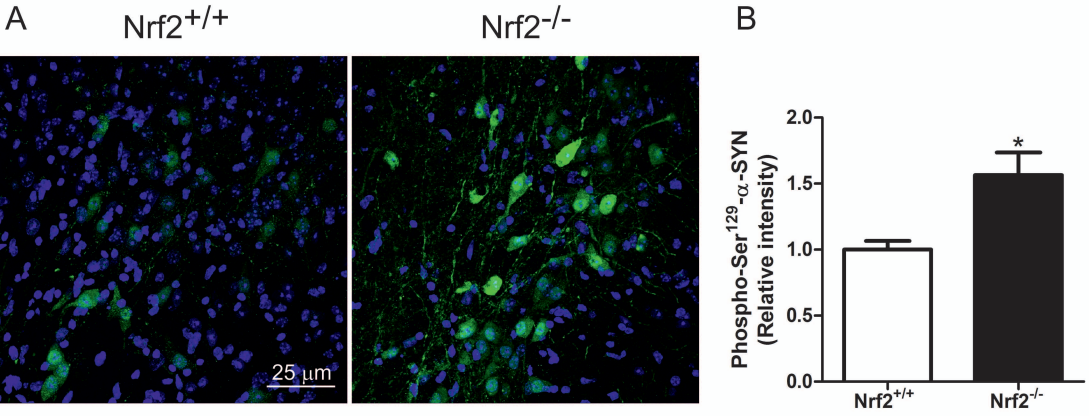
A
Nrf2+/+
Nrf2-/-
25 µm
B
Phospho-Ser129-α-SYN
(Relative intensity)
2.0
1.5
1.0
0.5
0.0
*
Nrf2+/+
Nrf2-/-

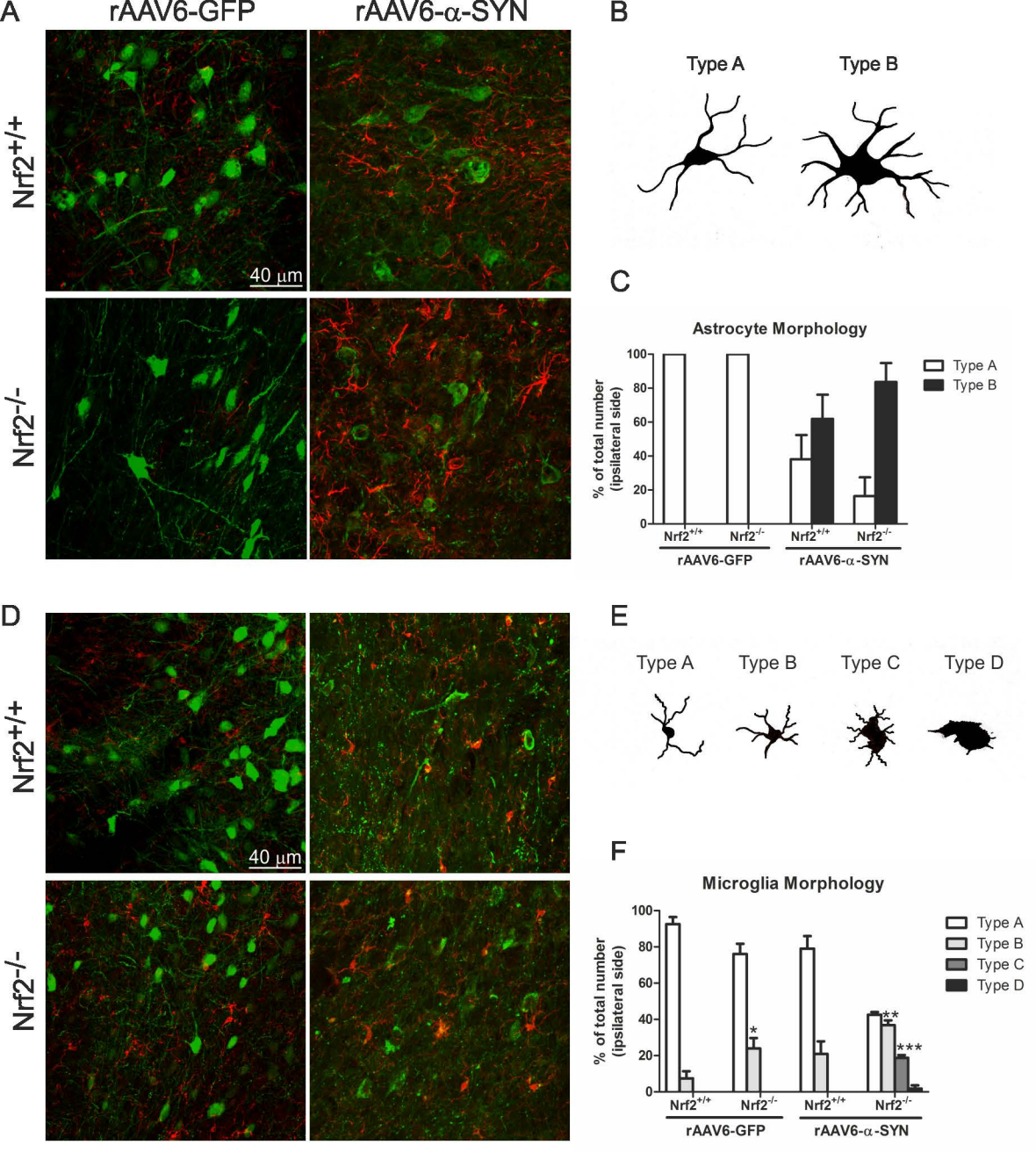
A
rAAV6-GFP
rAAV6-α-SYN
Nrf2+/+
Nrf2-/-
40 μm
B
Type A
Type B
C
Astrocyte Morphology
% of total number (ipsilateral side)
Type A
Type B
Nrf2+/+
Nrf2-/-
rAAV6-GFP
rAAV6-α-SYN
D
E
Type A
Type B
Type C
Type D
F
Microglia Morphology
*
**
***

GFAP
α-SYN
Merge
Nrf2+/+
Untreated
α-SYN
30 μm
Nrf2-/-
Untreated
α-SYN

Figure 7

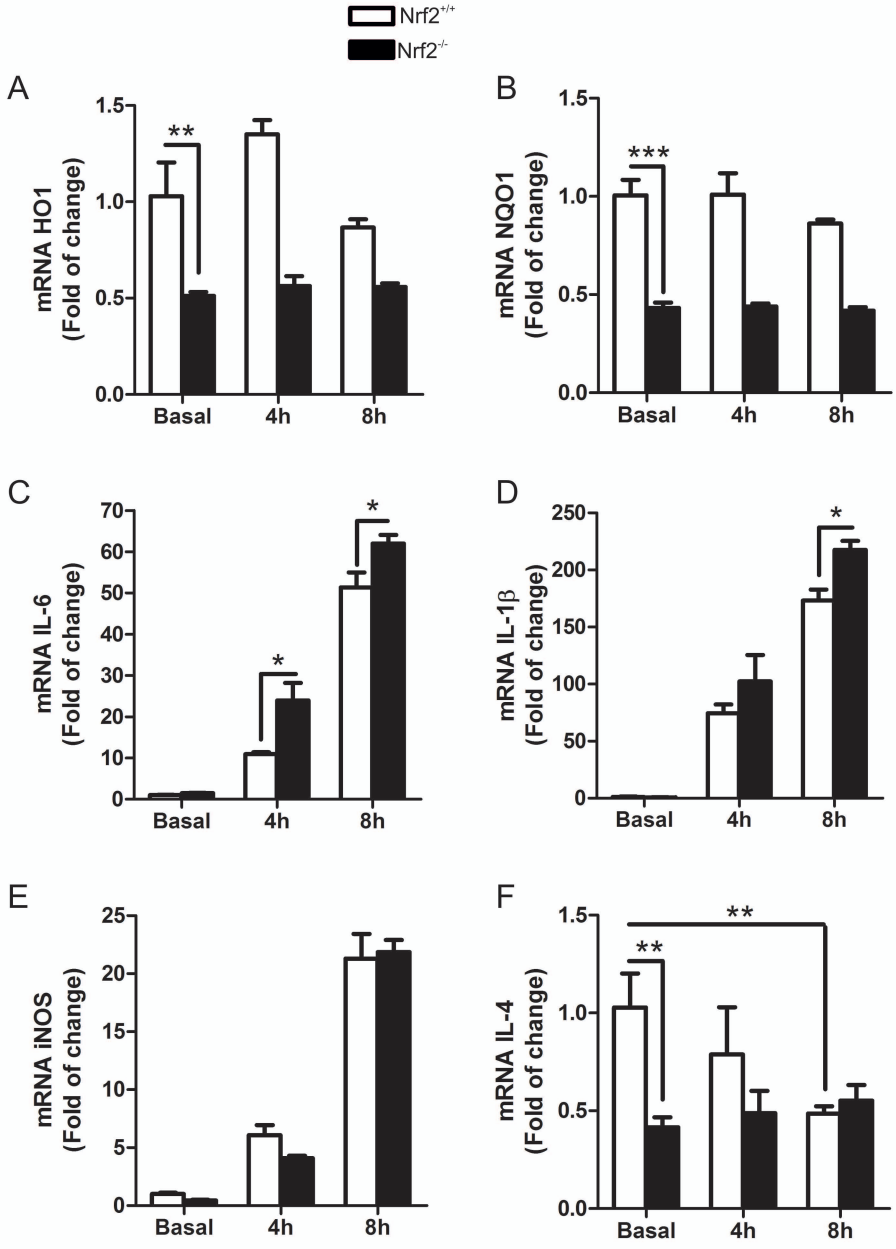
Nrf2+/+
Nrf2-/-
A
mRNA HO1 (Fold of change)
1.5
1.0
0.5
0.0
**
Basal
4h
8h
B
mRNA NQO1 (Fold of change)
1.5
1.0
0.5
0.0
***
Basal
4h
8h
C
mRNA IL-6 (Fold of change)
70
60
50
40
30
20
10
0
*
*
Basal
4h
8h
D
mRNA IL-1β (Fold of change)
250
200
150
100
50
0
*
Basal
4h
8h
E
mRNA iNOS (Fold of change)
25
20
15
10
5
0
Basal
4h
8h
F
mRNA IL-4 (Fold of change)
1.5
1.0
0.5
0.0
**
**
Basal
4h
8h

Figure 8

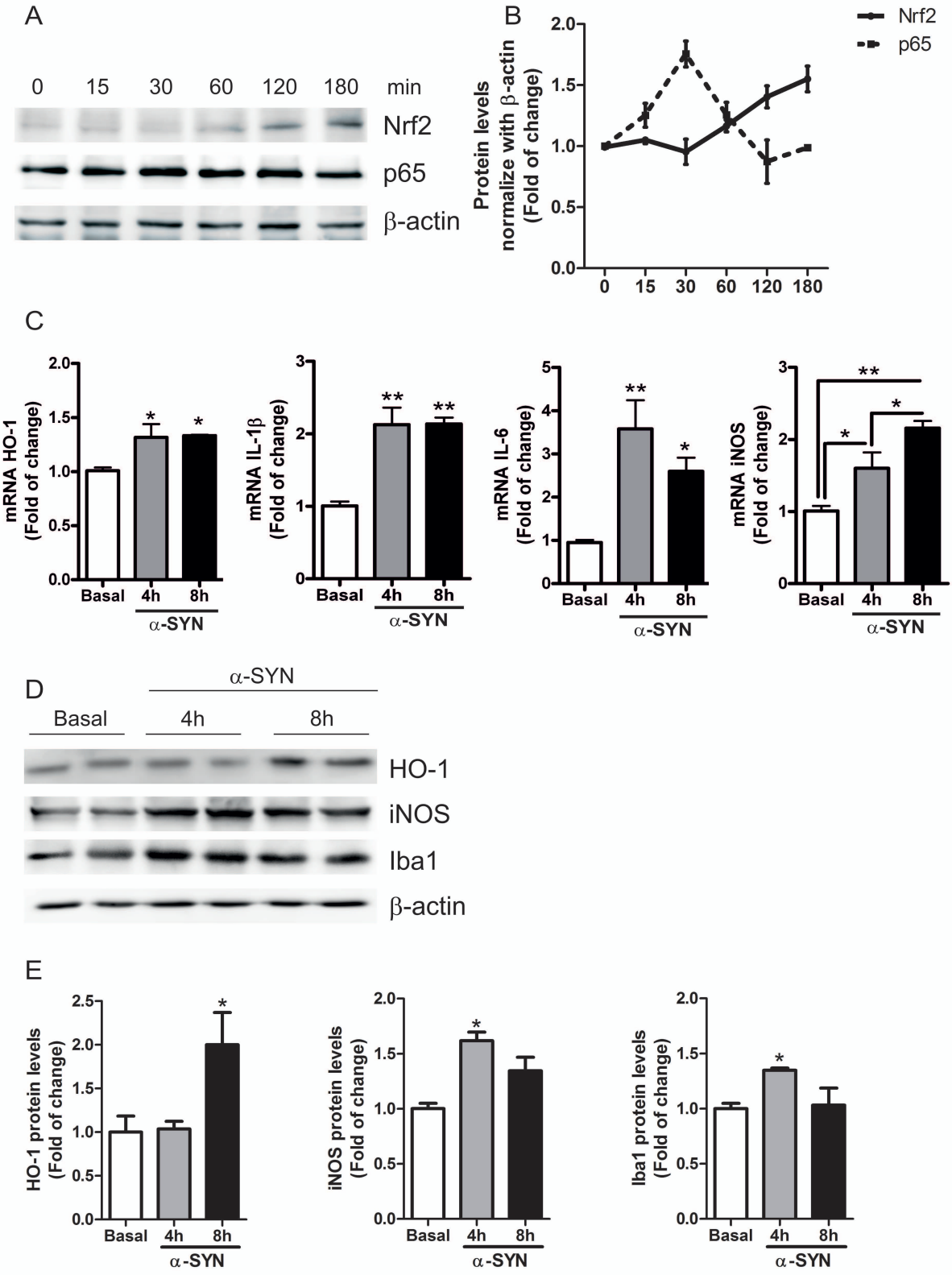
A
0
15
30
60
120
180
min
Nrf2
p65
β-actin
B
Nrf2
p65
Protein levels normalize with β-actin (Fold of change)
C
mRNA HO-1 (Fold of change)
mRNA IL-1β (Fold of change)
mRNA IL-6 (Fold of change)
mRNA iNOS (Fold of change)
Basal
4h
8h
α-SYN
D
α-SYN
Basal
4h
8h
HO-1
iNOS
Iba1
β-actin
E
HO-1 protein levels (Fold of change)
iNOS protein levels (Fold of change)
Iba1 protein levels (Fold of change)

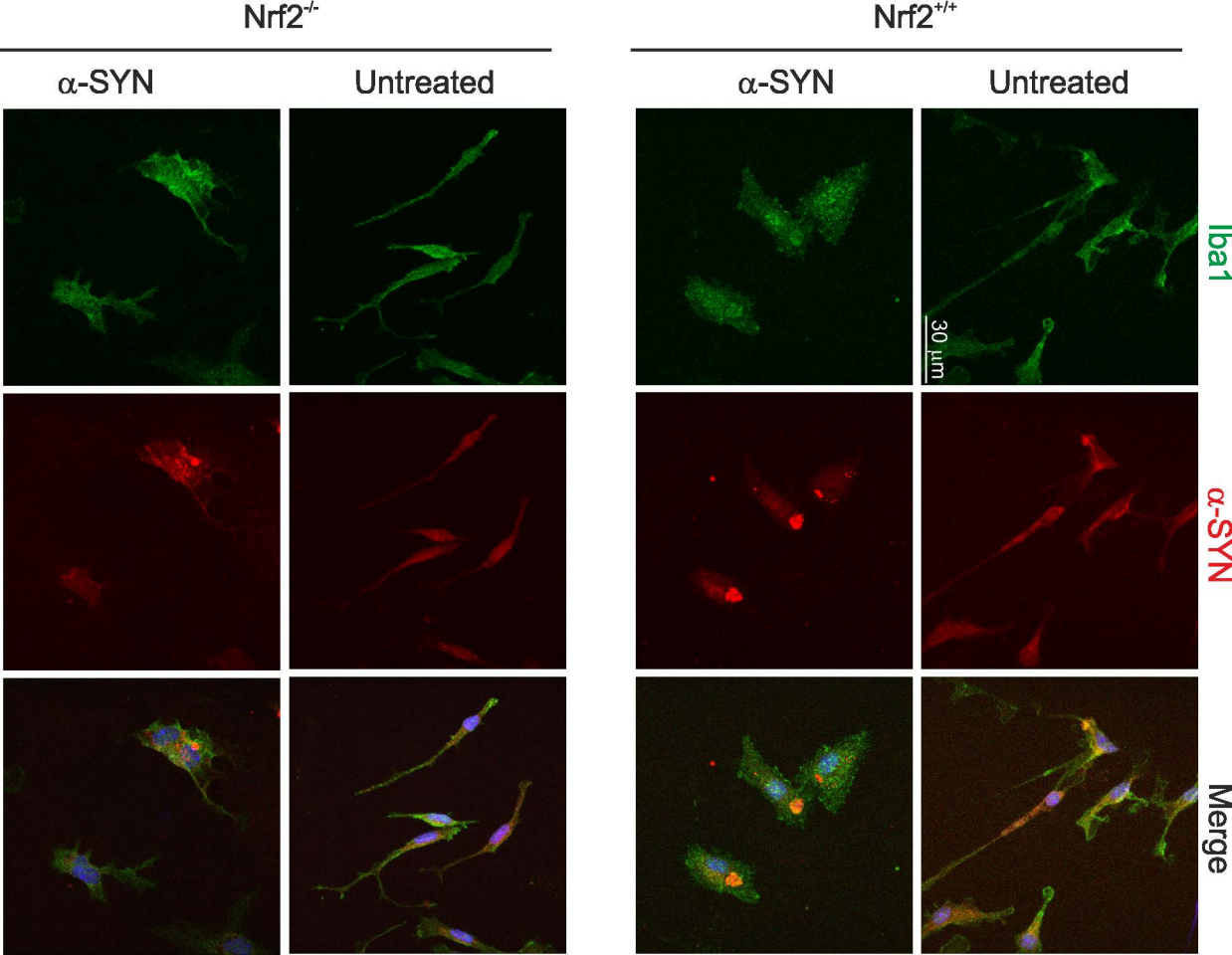
Nrf2-/-
Nrf2+/+
α-SYN
Untreated
α-SYN
Untreated
Iba1
α-SYN
Merge
30 μm

Figure 10

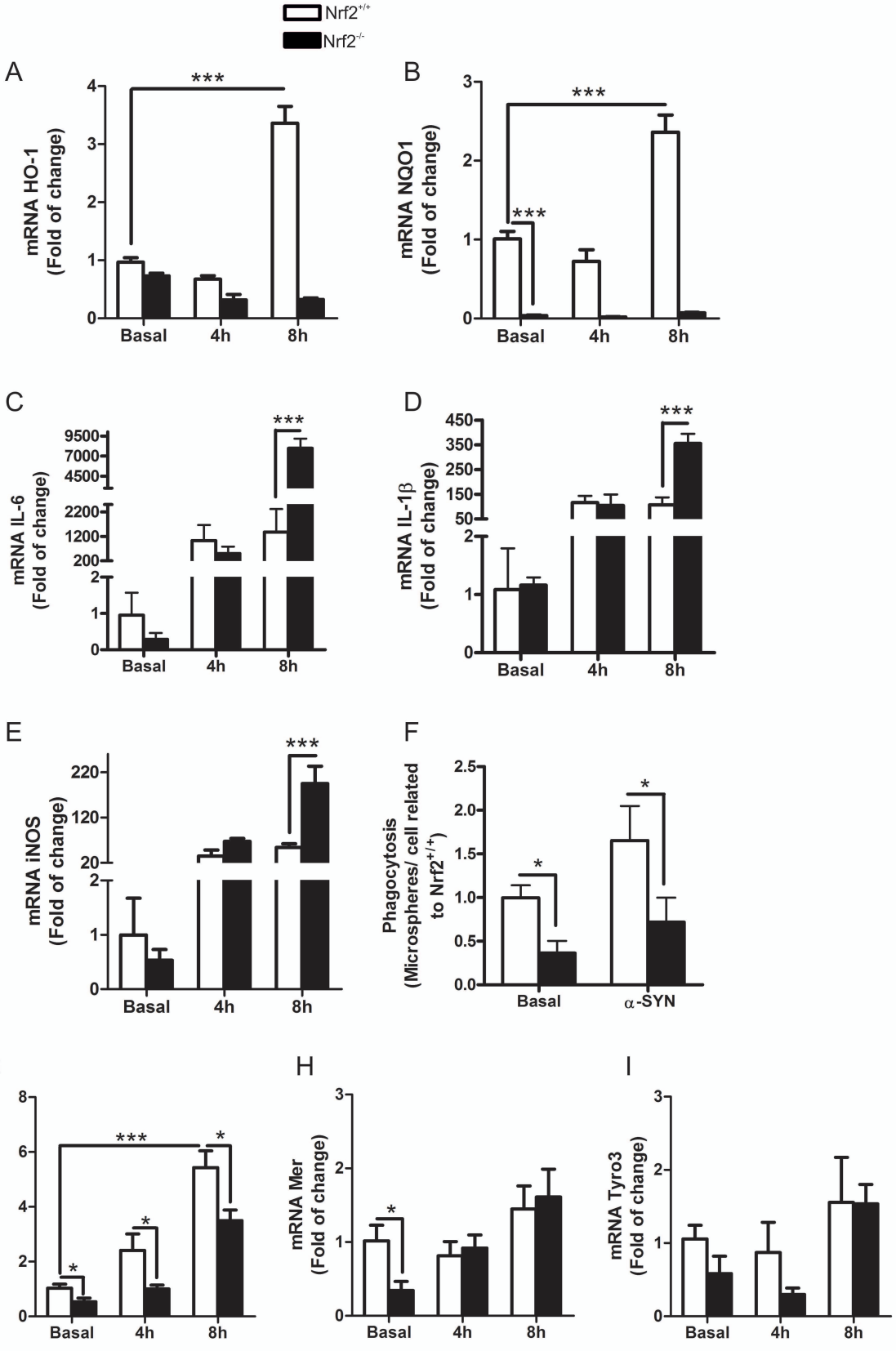
Nrf2+/+
Nrf2-/-
A
mRNA HO-1 (Fold of change)
***
Basal
4h
8h
B
mRNA NQO1 (Fold of change)
***
***
C
mRNA IL-6 (Fold of change)
***
D
mRNA IL-1β (Fold of change)
***
E
mRNA iNOS (Fold of change)
***
F
Phagocytosis (Microspheres/ cell related to Nrf2+/+)
*
*
α-SYN
G
mRNA Axl (Fold of change)
***
*
*
*
H
mRNA Mer (Fold of change)
*
I
mRNA Tyro3 (Fold of change)

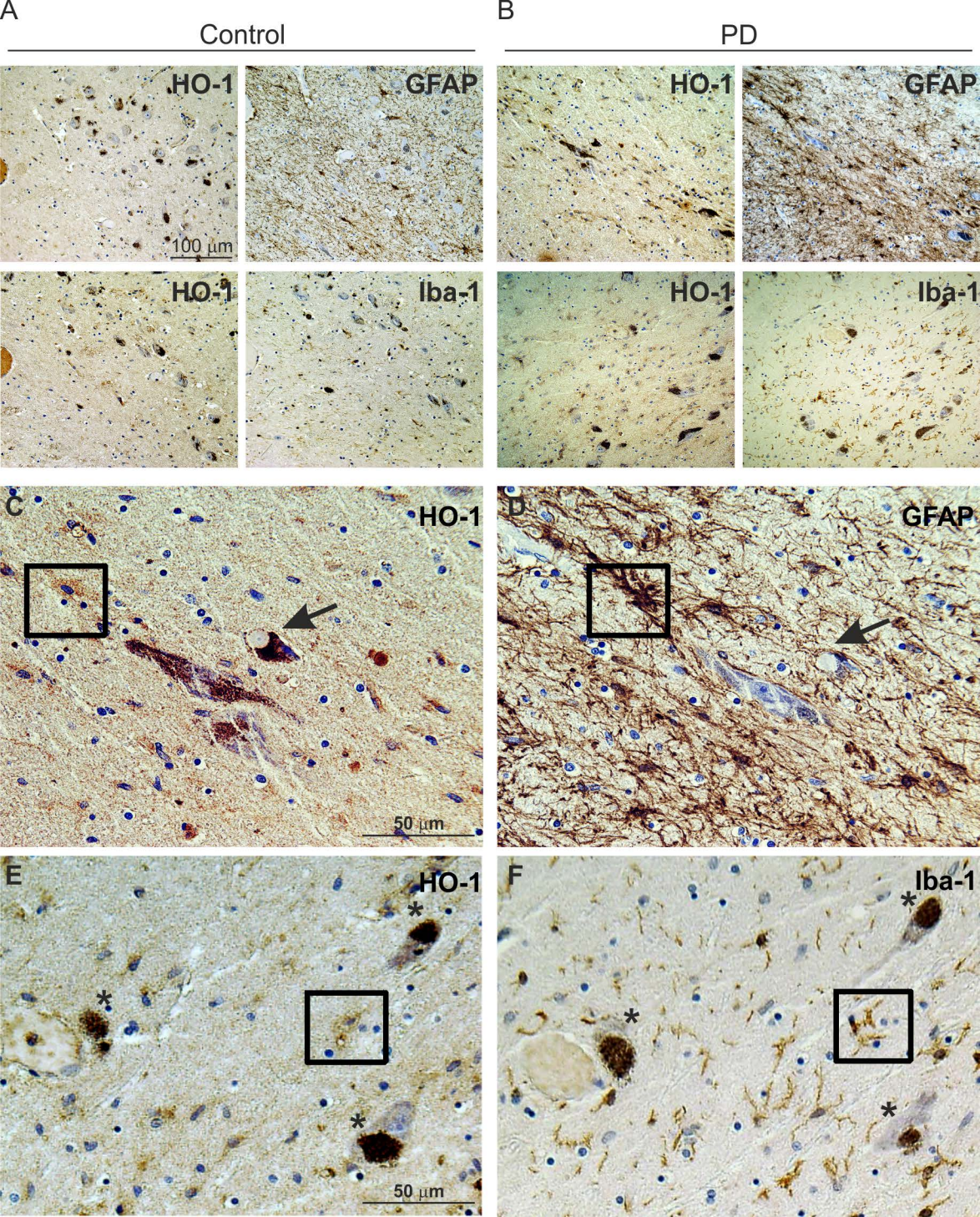
A
Control
B
PD
HO-1
GFAP
100 μm
HO-1
Iba-1
HO-1
GFAP
HO-1
Iba-1
C
HO-1
50 μm
D
GFAP
E
HO-1
50 μm
F
Iba-1

Figure 12

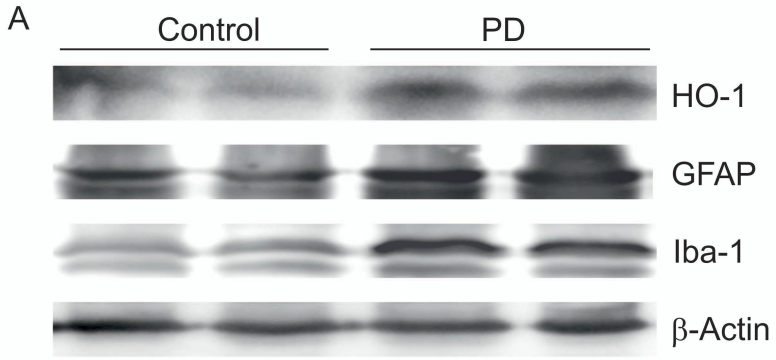
A
Control
PD
HO-1
GFAP
Iba-1
β-Actin
B
HO-1 protein levels (Fold of change)
2.0
1.5
1.0
0.5
0.0
**
Control
PD
Iba1 protein levels (Fold of change)
3
2
1
0
*
Control
PD
GFAP protein levels (Fold of change)
2.5
2.0
1.5
1.0
0.5
0.0
*
Control
PD

TABLE I. *Genes and primers for quantitative PCR amplification*

| Gene Product | Forward Primer | Reverse Primer |
|---|---|---|
| Axl | 5′ CGTGGCCTTGGTGGTATGTACTG 3′ | 5′ CTTTCCACGGTTGGCTCAAACAC 3′ |
| IL-1β | 5′ CTGGTGTGTGACGTTCCCATTA 3′ | 5′ CCGACAGCACGAGGCTTT 3′ |
| IL-4 | 5′ ACAGGAGAAGGGACGCCAT 3′ | 5′ GAAGCCCTACAGACGAGCTCA 3′ |
| IL-6 | 5′ CCTACCCCAATTTCCAATGCT 3′ | 5′ TATTTTCTGACCACAGTGAGGAATG 3′ |
| iNOS | 5′ CCTCCTTTGCCTCTCACTCTTC 3′ | 5′ AGTATTAGAGCGGTGGCATGGT 3′ |
| HO-1 | 5′ CACAGATGGCGTCACTTCGTC 3′ | 5′ GTGAGGACCCACTGGAGGAG 3′ |
| Mer | 5′ TGGTGGGCTACCGGATATCTCAC 3′ | 5′ CTGTGCAGGTGGCATTGTGGAT 3′ |
| NQO1 | 5′ GGTAGCGGCTCCATGTACTC 3′ | 5′ CATCCTTCCAGGATCTGCAT 3′ |
| PSMB7 | 5′ TCTTCGTCCATTCTCAGTGCC 3′ | 5′ GTAACTTTCTCGGTGAGGACAGC 3′ |
| PSMC3 | 5′ GCTCGGTGCACTGATGACTTC 3′ | 5′ CATGAGTGAGTTCCGTGGCTC 3′ |
| PSMC4 | 5′ GGCCCGTCCAGATAAGATTTC 3′ | 5′ TCCTTGGCCAGGACAATGTAG 3′ |
| Tyro3 | 5′ GTTCACCCTCGGTCGGATGTTG 3′ | 5′ GTCGCTTGAGGCAATGATGTCAG 3′ |
| β-actin | 5′ TCCTTCCTGGGCATGGAG 3′ | 5′ AGGAGGAGCAATGATCTTGATCTT 3′ |

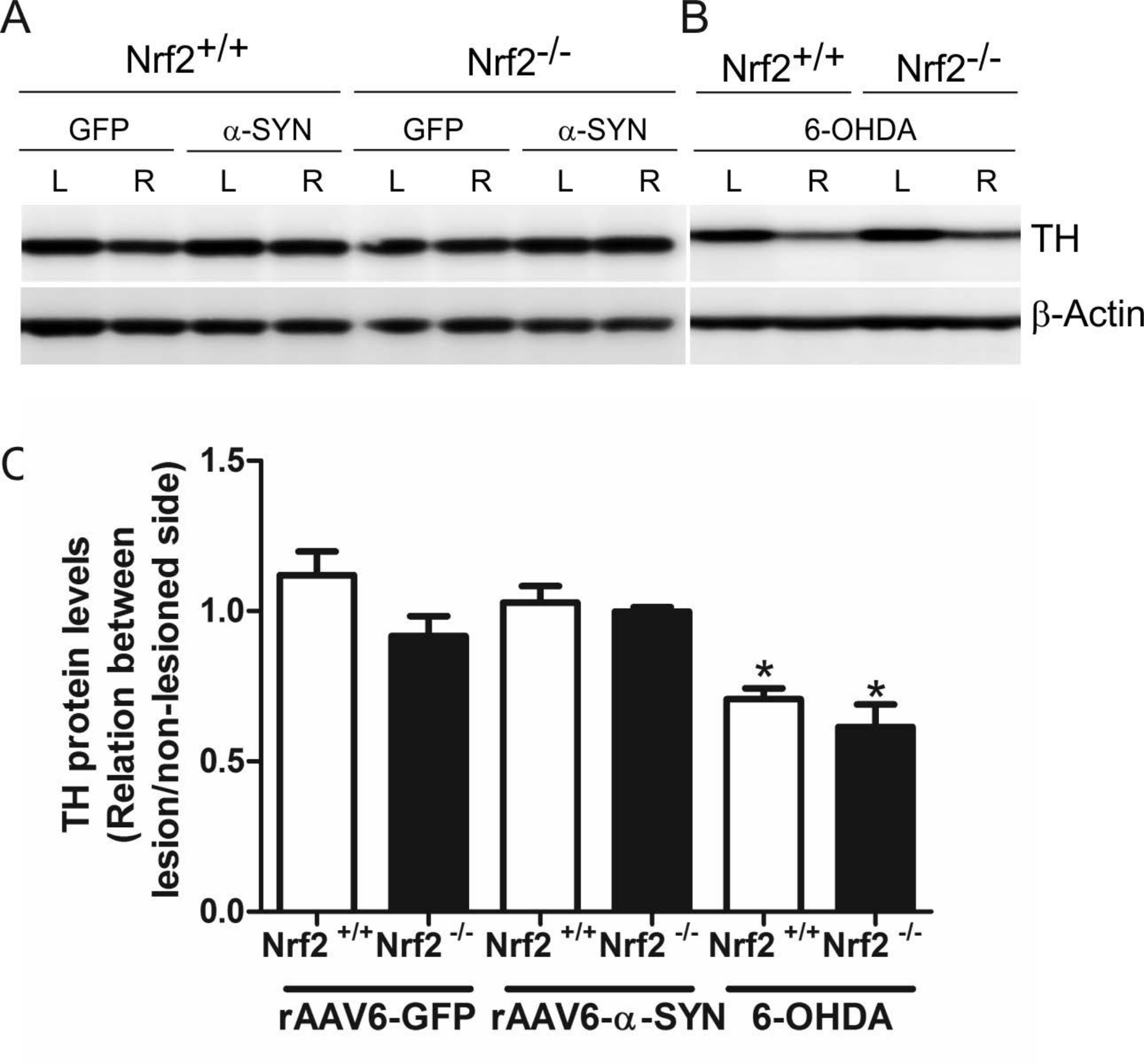
A
Nrf2+/+
Nrf2-/-
GFP
α-SYN
GFP
α-SYN
L
R
L
R
L
R
L
R
B
Nrf2+/+
Nrf2-/-
6-OHDA
L
R
L
R
TH
β-Actin
C
TH protein levels
(Relation between
lesion/non-lesioned side)
1.5
1.0
0.5
0.0
*
*
Nrf2 +/+
Nrf2 -/-
Nrf2 +/+
Nrf2 -/-
Nrf2 +/+
Nrf2 -/-
rAAV6-GFP
rAAV6-α-SYN
6-OHDA

Suppl. Figure 1

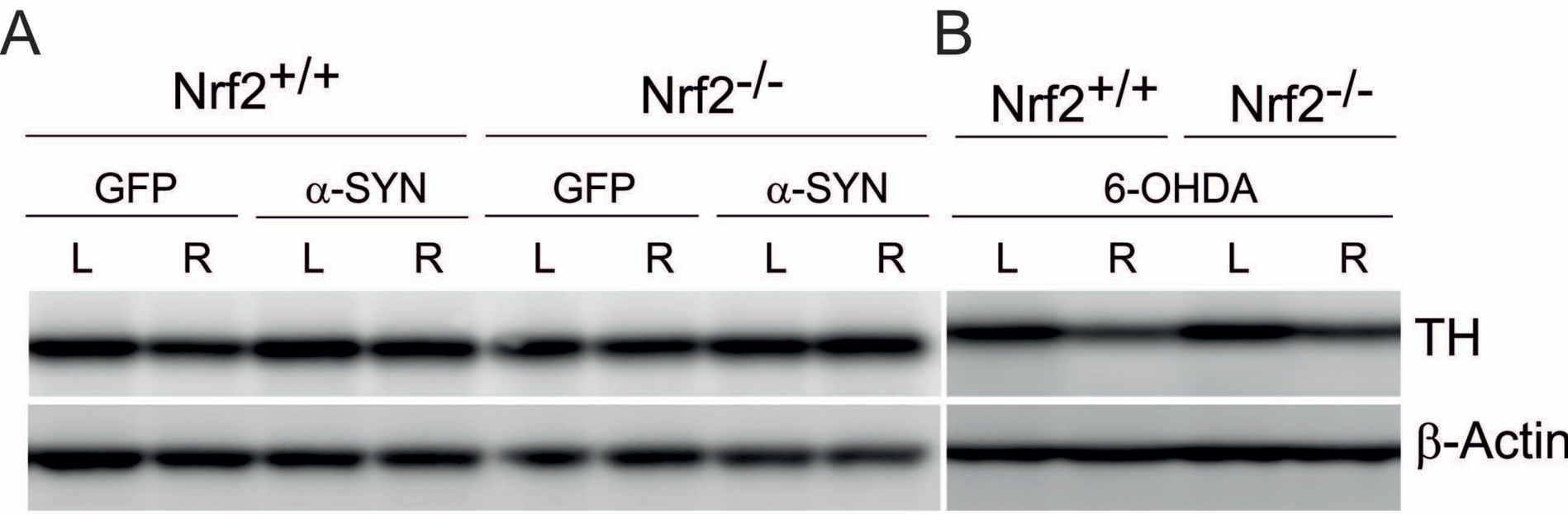


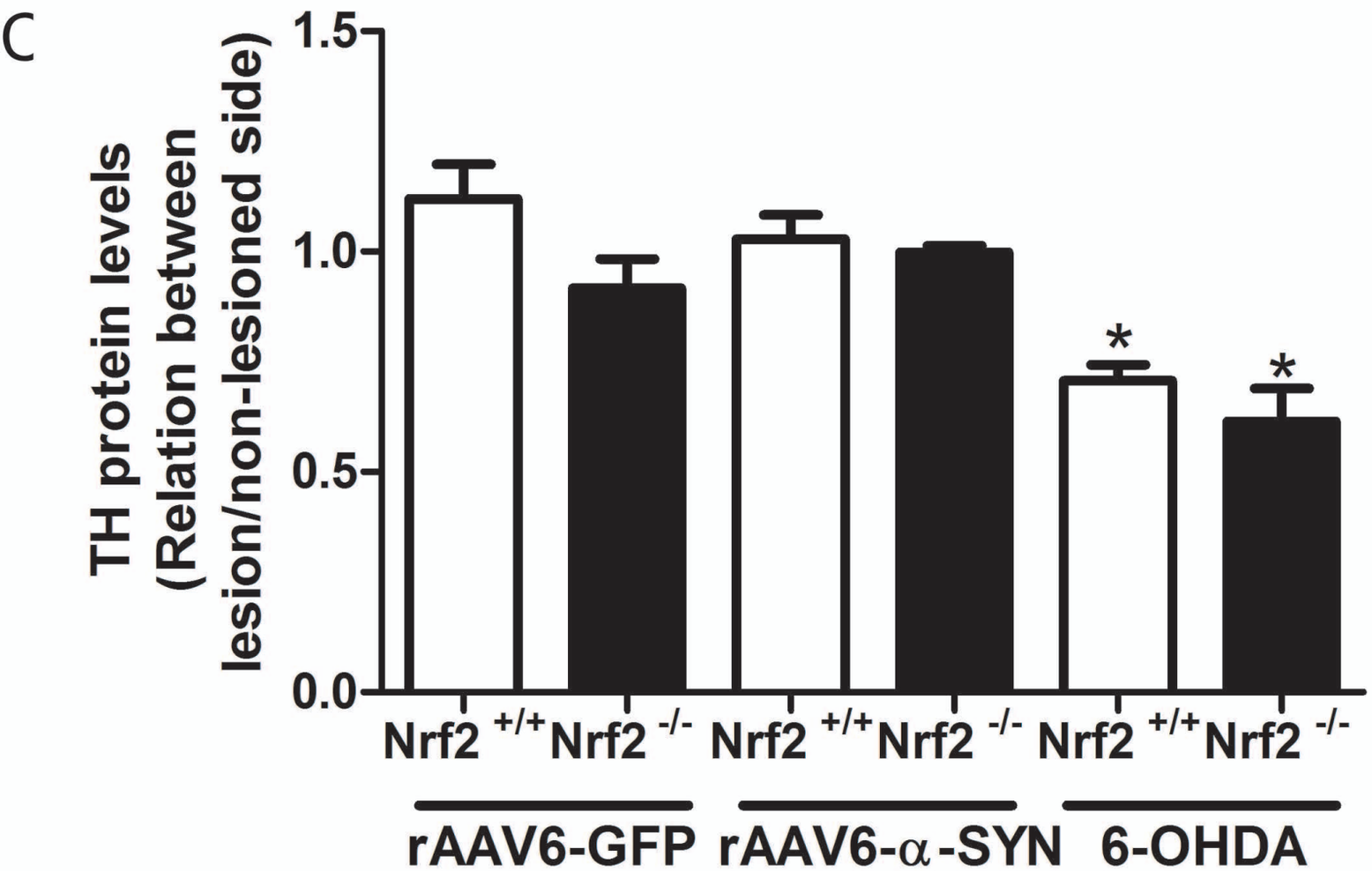

Suppl. Figure 2

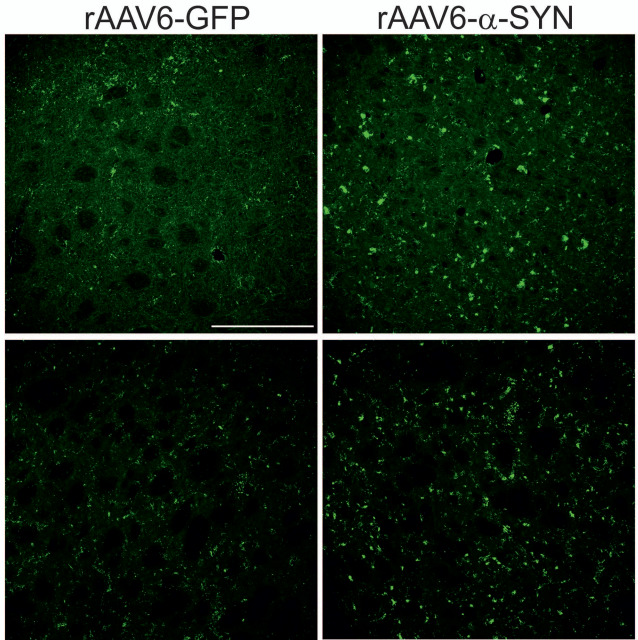


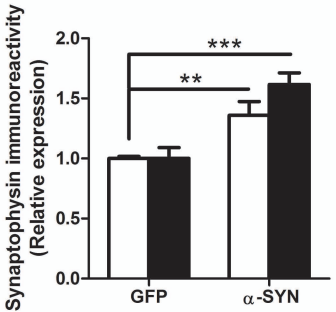

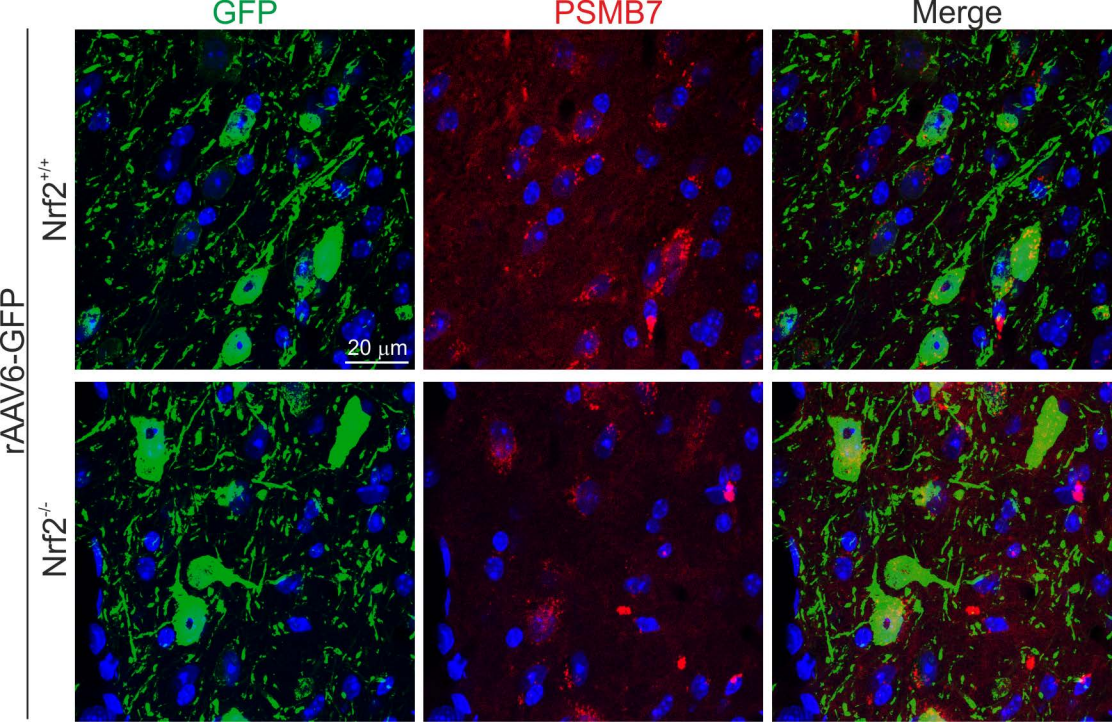
GFP
PSMB7
Merge
rAAV6-GFP
Nrf2+/+
Nrf2-/-
20 μm

Suppl. Figure 4

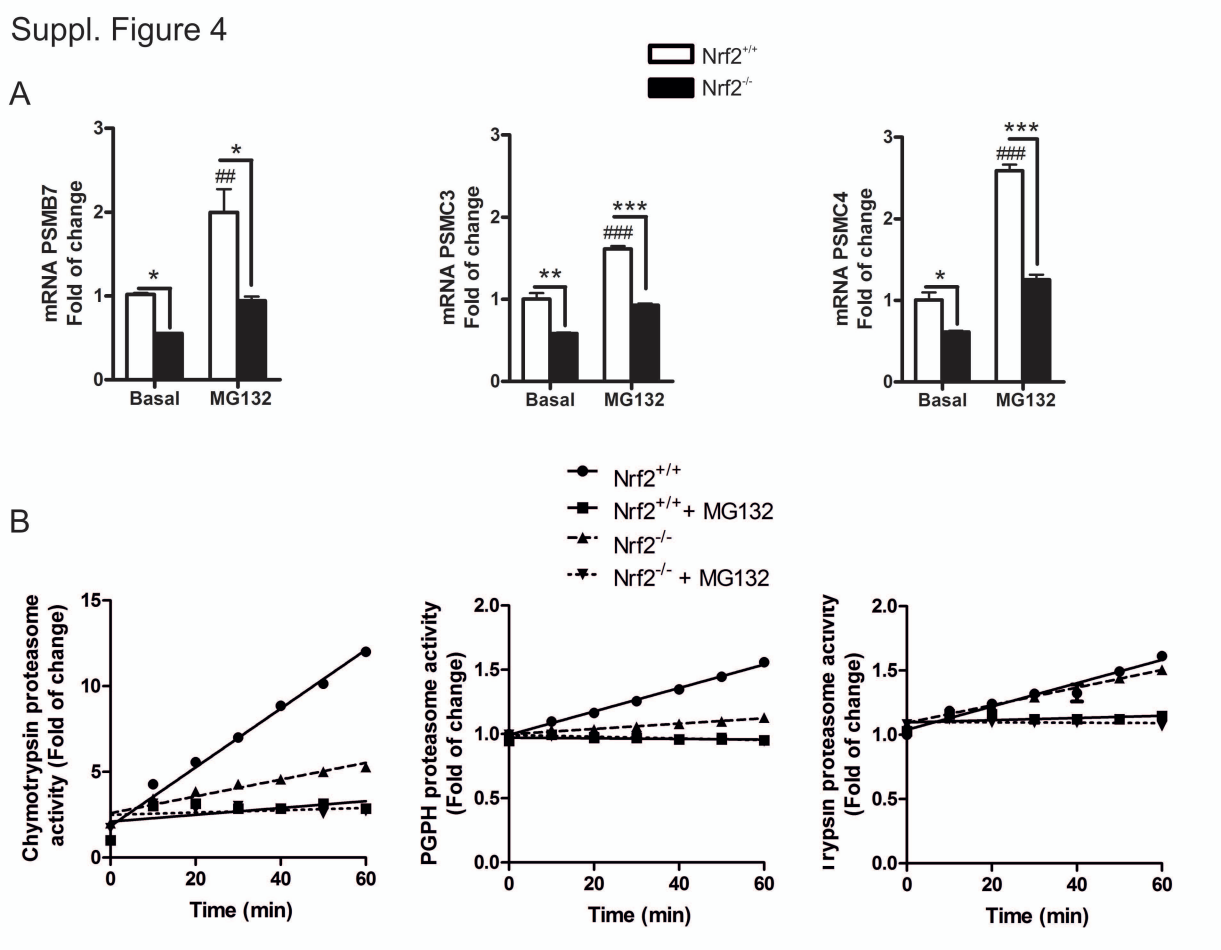

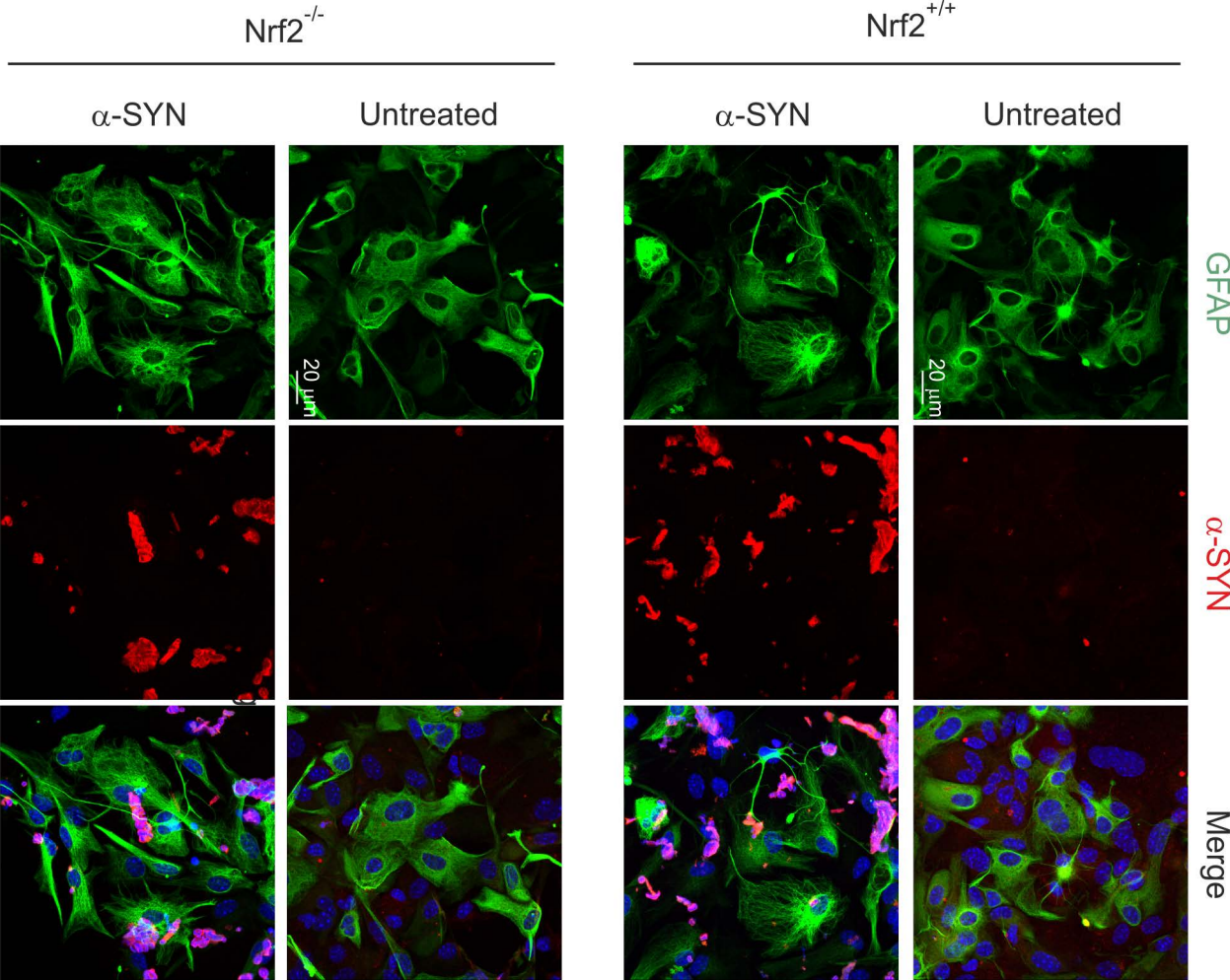
Nrf2-/-
Nrf2+/+
α-SYN
Untreated
α-SYN
Untreated
20 μm
20 μm
GFAP
α-SYN
Merge

Suppl. Figure 6